

Tensor-train methods for sequential state and parameter learning in state-space models

Yiran Zhao

Tiangang Cui

*School of Mathematics, Monash University
Victoria 3800, Australia*

YIRAN.ZHAO@MONASH.EDU

TIANGANG.CUI@MONASH.EDU

Editor:

Abstract

We consider sequential state and parameter learning in state-space models with intractable state transition and observation processes. By exploiting low-rank tensor-train (TT) decompositions, we propose new sequential learning methods for joint parameter and state estimation under the Bayesian framework. Our key innovation is the introduction of scalable function approximation tools such as TT for recursively learning the sequentially updated posterior distributions. The function approximation perspective of our methods offers tractable error analysis and potentially alleviates the particle degeneracy faced by many particle-based methods. In addition to the new insights into algorithmic design, our methods complement conventional particle-based methods. Our TT-based approximations naturally define conditional Knothe–Rosenblatt (KR) rearrangements that lead to filtering, smoothing and path estimation accompanying our sequential learning algorithms, which open the door to removing potential approximation bias. We also explore several preconditioning techniques based on either linear or nonlinear KR rearrangements to enhance the approximation power of TT for practical problems. We demonstrate the efficacy and efficiency of our proposed methods on several state-space models, in which our methods achieve state-of-the-art estimation accuracy and computational performance.

Keywords: tensor train, Knothe–Rosenblatt rearrangement, state-space models, sequential Monte Carlo, uncertainty quantification, transport maps

1 Introduction

State-space models have been widely used in mathematical and statistical modeling to analyze time-varying complex phenomena (Cappé et al., 2006; Kantas et al., 2009). Examples include time series analysis in finance, temporal pattern recognition in bioinformatics, forecast in meteorology, and more. A typical state-space model is also referred to as a hidden Markov model, which consists of two stochastic processes, $\{\mathbf{X}_t\}_{t \geq 0}$ and $\{\mathbf{Y}_t\}_{t \geq 1}$. The state transition process $\{\mathbf{X}_t\}_{t \geq 0}$ is an \mathcal{X} -valued latent Markov process specified by a conditional transition density

$$(\mathbf{X}_t | \mathbf{X}_{0:t-1} = \mathbf{x}_{0:t-1}) \equiv (\mathbf{X}_t | \mathbf{X}_{t-1} = \mathbf{x}_{t-1}) \sim f(\mathbf{x}_t | \mathbf{x}_{t-1}, \boldsymbol{\theta}) \quad (1)$$

and an initial density $p(\mathbf{x}_0 | \boldsymbol{\theta})$. Here \mathbf{X}_t represents the hidden state of the underlying system at an integer-valued time index $t \geq 0$ and the notation $\mathbf{x}_{i:j}$ denotes vectors $(\mathbf{x}_i, \mathbf{x}_{i+1}, \dots, \mathbf{x}_j)$ of a sequence $\{\mathbf{x}_t\}_{t \geq 0}$. The \mathcal{Y} -valued observation process $\{\mathbf{Y}_t\}_{t \geq 1}$ is characterized by the

likelihood function $g(\mathbf{y}_t|\mathbf{x}_t, \boldsymbol{\theta})$ as

$$(\mathbf{Y}_t|\mathbf{X}_{0:t} = \mathbf{x}_{0:t}, \mathbf{Y}_{1:t-1} = \mathbf{y}_{1:t-1}) \equiv (\mathbf{Y}_t|\mathbf{X}_t = \mathbf{x}_t) \sim g(\mathbf{y}_t|\mathbf{x}_t, \boldsymbol{\theta}), \quad (2)$$

where \mathbf{Y}_t represents observables at time index $t > 0$. In (1) and (2), $\boldsymbol{\theta} \in \Theta$ is a set of parameters that govern the state transition and observation processes.

Example 1 (*Volatility of financial derivatives.*) The stochastic volatility model consists of the logarithm of the volatility $\{\mathbf{X}_t\}_{t \geq 0}$ and the return of an asset $\{\mathbf{Y}_t\}_{t \geq 1}$. In the simplest setup, the log-volatility $\{\mathbf{X}_t\}_{t \geq 0}$ is a scalar-valued autoregressive process with order 1, i.e., an AR(1) process, while the scalar-valued return $\{\mathbf{Y}_t\}_{t \geq 1}$ is the observable determined by the volatility. The system is described by

$$\begin{cases} \mathbf{X}_t = \gamma \mathbf{X}_{t-1} + \sigma \varepsilon_t^{(x)} \\ \mathbf{Y}_t = \varepsilon_t^{(y)} \beta \exp(\frac{1}{2} \mathbf{X}_t) \end{cases},$$

where $\boldsymbol{\Theta} = (\gamma, \sigma, \beta)$ are model parameters, $\varepsilon_t^{(x)}$ and $\varepsilon_t^{(y)}$ are independent and identically distributed (i.i.d.) standard Gaussian random variables, and the initial state is given as $\mathbf{X}_0 \sim \mathcal{N}(0, \frac{\sigma^2}{1-\gamma^2})$. The goal is to estimate the parameter $\boldsymbol{\Theta}$ and the hidden states $\{\mathbf{X}_t\}_{t \geq 0}$ from observed return $\{\mathbf{Y}_t\}_{t \geq 1}$.

1.1 Sequential learning problems

Following the state-space model defined in (1) and (2), random variables $(\boldsymbol{\Theta}, \mathbf{X}_{0:t}, \mathbf{Y}_{1:t})$ have the joint density

$$p(\boldsymbol{\theta}, \mathbf{x}_{0:t}, \mathbf{y}_{1:t}) = p(\boldsymbol{\theta}) p(\mathbf{x}_0|\boldsymbol{\theta}) \prod_{j=1}^t \left(f(\mathbf{x}_j|\mathbf{x}_{j-1}, \boldsymbol{\theta}) g(\mathbf{y}_j|\mathbf{x}_j, \boldsymbol{\theta}) \right), \quad (3)$$

where $p(\boldsymbol{\theta})$ and $p(\mathbf{x}_0|\boldsymbol{\theta})$ are prescribed prior densities. Conditioned on all available data $\mathbf{Y}_{1:t} = \mathbf{y}_{1:t}$ at time t , the trajectory of the states $\mathbf{X}_{0:t}$ and the parameter $\boldsymbol{\Theta}$ jointly follow the posterior density

$$p(\boldsymbol{\theta}, \mathbf{x}_{0:t}|\mathbf{y}_{1:t}) = \frac{p(\boldsymbol{\theta}, \mathbf{x}_{0:t}, \mathbf{y}_{1:t})}{p(\mathbf{y}_{1:t})}, \quad (4)$$

where $p(\mathbf{y}_{1:t})$ is an unknown constant commonly referred to as the evidence. We aim to design sequential algorithms that simultaneously solve the following inference problems at each time t :

- **Filtering.** Estimating the current state, which is the marginal conditional random variable

$$(\mathbf{X}_t|\mathbf{Y}_{1:t} = \mathbf{y}_{1:t}) \sim p(\mathbf{x}_t|\mathbf{y}_{1:t}) := \int p(\boldsymbol{\theta}, \mathbf{x}_{0:t}|\mathbf{y}_{1:t}) d\mathbf{x}_{0:t-1} d\boldsymbol{\theta}. \quad (5)$$

- **Parameter estimation.** Estimating the unknown parameter, which is the marginal conditional random variable

$$(\boldsymbol{\theta}|\mathbf{Y}_{1:t} = \mathbf{y}_{1:t}) \sim p(\boldsymbol{\theta}|\mathbf{y}_{1:t}) := \int p(\boldsymbol{\theta}, \mathbf{x}_{0:t}|\mathbf{y}_{1:t}) d\mathbf{x}_{0:t}. \quad (6)$$

- **Path estimation.** Estimating the trajectory of states, which are the marginal conditional random variables

$$(\mathbf{X}_{0:t} | \mathbf{Y}_{1:t} = \mathbf{y}_{1:t}) \sim p(\mathbf{x}_{0:t} | \mathbf{y}_{1:t}) := \int p(\boldsymbol{\theta}, \mathbf{x}_{0:t} | \mathbf{y}_{1:t}) d\boldsymbol{\theta}. \quad (7)$$

- **Smoothing.** As a result of increasing state dimensions and observation size, path estimation becomes increasingly challenging over time. Smoothing is a related learning problem focusing on the lower-dimensional marginal conditional random variable

$$(\mathbf{X}_k | \mathbf{Y}_{1:t} = \mathbf{y}_{1:t}) \sim p(\mathbf{x}_k | \mathbf{y}_{1:t}) := \int p(\boldsymbol{\theta}, \mathbf{x}_{0:t} | \mathbf{y}_{1:t}) d\mathbf{x}_{0:k-1} d\mathbf{x}_{k+1:t} d\boldsymbol{\theta} \quad (8)$$

for some previous time index $k < t$.

In the presence of unknown parameters and stochastic noises in the state transition (1), all the abovementioned learning problems are essentially characterizations of marginal random variables. Furthermore, the random variables of interest are intractable, in the sense that the characteristic functions and moments often do not admit analytical forms, and the direct simulation of these random variables is not feasible. Thus, we need to design numerical methods to solve these problems. In principle, algorithms for solving these problems need to be *sequential* by design—the computation of new solutions to the problems (5)–(8) at time t only relies on either previous solutions at $t - 1$ for forward algorithms, or solutions at $t + 1$ for backward algorithms. We refer readers to Evensen et al. (2022); Kantas et al. (2009); Reich and Cotter (2015) and Särkkä (2013) for further details and references of these sequential learning problems.

1.2 Related work

Assuming the parameter $\boldsymbol{\theta}$ is known, the classical filtering problem aims to estimate the current state $(\mathbf{X}_t | \boldsymbol{\Theta} = \boldsymbol{\theta}, \mathbf{Y}_{1:t} = \mathbf{y}_{1:t})$ conditioned on the data available up to t . For linear models with Gaussian noises, the filtering density yields a closed-form solution given by the classical Kalman filter (Kalman, 1960). The Kalman filter sequentially updates the mean and covariance of the Gaussian filtering density using a Kalman gain matrix when new observations become available. The extended Kalman filter and its variants (Anderson and Moore, 2012; Einicke and White, 1999) generalize the Kalman filter to nonlinear models by linearizing state transition processes. The ensemble Kalman filter (Evensen, 2003) bypasses the linearization but adopts Gaussian assumptions to approximate the Kalman gain matrix using Monte Carlo sampling. This makes the ensemble Kalman filter flexible to implement and robust with respect to dimensionality. However, the linearization and Gaussian assumptions used by extended and ensemble Kalman filters introduce unavoidable approximation errors to the resulting filtering density, which makes them only suitable for tracking the states.

Sequential Monte Carlo (SMC) methods are widely used to fully characterize the sequentially updated filtering density (5) in general nonlinear problems. In the simplest form, the bootstrap filter (Gordon et al., 1993) sequentially updates a set of weighted state samples using the state transition process, and reweights the samples using the likelihood function once new data are collected. One major problem of the bootstrap filter is that the weights

tend to degenerate over time, known as particle degeneracy (Doucet and Johansen, 2009; Snyder et al., 2008; Liu et al., 2001; Pitt and Shephard, 1999). To mitigate particle degeneracy, the auxiliary particle filter (Pitt and Shephard, 1999, 2001) and various advanced resampling techniques such as residual resampling (Carpenter et al., 1999), systematic resampling (Kitagawa, 1996) and resample-move (Gilks and Berzuini, 2001) are developed. See Del Moral et al. (2012); Doucet and Johansen (2009); Reich and Cotter (2015) and Maskell and Gordon (2002) for comprehensive reviews of these techniques.

An emerging trend is the development of transport map methods that overcome the particle degeneracy by transforming the forecast particles into equally weighted particles following the filtering density. The ensemble transform filter (Reich, 2013) maps the particles by solving a discrete optimal transport problem, in which the transformation is guided by one step of importance sampling for sketching the updated filtering density. The coupling technique of Spantini et al. (2022) generalizes the ensemble Kalman filter beyond the Gaussian assumption, in which the mapping of particles is achieved via conditional transforms—trained by solving optimization problems—rather than importance sampling. The implicit sampling method (Chorin and Tu, 2009; Morzfeld et al., 2012) defines implicit transport maps from some reference densities, e.g., a standard Gaussian, to a particular approximation of the filtering density. Methods based on neural networks are also considered. For example, Gottwald and Reich (2021) build random feature maps on delayed coordinates to accelerate filtering, and Hoang et al. (2021) approximate conditional mean filters using artificial neural networks.

With known parameter $\boldsymbol{\theta}$, the smoothing problem aiming at $(\mathbf{X}_k|\boldsymbol{\Theta} = \boldsymbol{\theta}, \mathbf{Y}_{1:t} = \mathbf{y}_{1:t})$ for $k < t$ can be solved by the forward-backward smoother (Godsill et al., 2004), which reweights and resamples particles drawn from $(\mathbf{X}_t|\boldsymbol{\Theta} = \boldsymbol{\theta}, \mathbf{Y}_{1:t} = \mathbf{y}_{1:t})$ —i.e., solutions to the filtering problem—backward from \mathbf{X}_t to \mathbf{X}_k . More advanced methods such as the generalized two-filter smoothing—e.g., Bresler (1986); Briers et al. (2010) and Fearnhead et al. (2010)—are also developed. Those methods run a backward particle filter with carefully chosen proposal distributions to generate entire (weighted) state paths. Certain state-space models have a “forgetting” nature in the sense that the current state \mathbf{x}_t has negligible impact on data observed after $t + \Delta$ for some lag $\Delta > 0$. In this case, one can also apply the fixed-lag strategy (Kitagawa and Sato, 2001; Olsson et al., 2008) to approximate the target smoothing density using $p(\mathbf{x}_k|\boldsymbol{\theta}, \mathbf{y}_{k+\Delta})$. However, estimating a suitable lag Δ can be an art.

For systems with unknown parameters, characterizing the posterior parameter density (6) can be challenging as it requires marginalization over the state path. The particle Markov chain Monte Carlo (MCMC) method of Andrieu et al. (2010) employs a Markov chain transition kernel invariant to the marginal posterior density $p(\boldsymbol{\theta}|\mathbf{y}_{1:t})$ to simulate posterior parameter random variables. To calculate the computationally intractable marginal posterior density $p(\boldsymbol{\theta}|\mathbf{y}_{1:t})$, the particle MCMC applies a particle filter over the state $\mathbf{X}_{0:t}$, associated with each parameter particle. As a byproduct, this method can simulate the joint posterior random variables $(\boldsymbol{\Theta}, \mathbf{X}_{0:t}|\mathbf{Y}_{1:t} = \mathbf{y}_{1:t})$, and thus can simultaneously solve the learning problems in (5)–(8). Similar methods include Särkkä et al. (2015) and Mbalawata et al. (2013), which deal with continuous-time state transition processes and approximate the marginal likelihood using various Gaussian filters. Overall, these methods are often designed for handling batched data, and thus may have difficulties in updating the solution in an online manner with newly observed data.

To enable online estimation of posterior parameters, the SMC² method (Chopin et al., 2013) runs an outer-loop particle filter to update the parameter distribution. Each of the parameter samples is associated with an inner-loop particle filter of the states, which estimates the density $p(\boldsymbol{\theta}|\mathbf{y}_{1:t})$. Within SMC², a particle MCMC method is used as a restart step whenever the effective sample size of the parameter particles drops below some threshold. Because of the particle MCMC rejuvenation step, the SMC² method is not purely recursive and has a computational complexity quadratically in time. The nested particle filter (Crisan and Miguez, 2018) uses a similar two-loop structure as SMC² and jittering kernels to update parameter particles instead of the rejuvenation step. The use of jittering kernels allows for recycling state particle filters associated with the old parameters, and thus achieves a reduced computational complexity linear in time. However, the target distribution of the jittering kernel is not invariant to the marginal posterior density $p(\boldsymbol{\theta}|\mathbf{y}_{1:t})$. As a result, the nested particle filter has a convergence rate of $N^{-1/4}$, where N is the sample size, which is lower than the $N^{-1/2}$ rate of the SMC² method.

1.3 Contributions and outline

We present a set of new methods for solving sequential state and parameter learning problems. Instead of using particle-based methods, the backbone of our methods is built upon the tensor-train (TT) decomposition (Hackbusch, 2012; Oseledets and Tyrtyshnikov, 2010; Oseledets, 2011), which is a scalable function approximation tool.

We propose in Section 2 a basic version of the TT-based algorithm that recursively approximates the time-varying joint posterior densities. The separable form of TT provides approximations to the marginal densities required in learning problems (5)–(8). The basic TT-based algorithm is useful to outline the design principles and key steps of our proposed methods. However, the rank truncation used by TT may not preserve the non-negativity of density functions. This leads to difficulties in removing the approximation bias using techniques such as importance sampling. We overcome this limitation in Section 3 by integrating the square-root approximation technique of Cui and Dolgov (2022) into the basic algorithm of Section 2. This preserves the recursive learning pattern of the basic algorithm for problems (5)–(8) and leads to non-negative approximation by construction. More importantly, the separable form of the non-negative TT naturally leads to a sequence of Knothe–Rosenblatt (KR) rearrangements (Knothe et al., 1957; Rosenblatt, 1952) that couple reference random variables and the marginal random variables of interest. We utilize the resulting (conditional) KR rearrangements to design particle filters and particle smoothers accompanying TT approximations to remove estimation bias.

The smoothing procedure accompanying our TT-based learning algorithm shares many similarities with the joint KR rearrangements developed in Spantini et al. (2018). In particular, our joint KR rearrangement for the simultaneous path and parameter estimation (see Section 3.4) follows the same sparsity pattern as that of Spantini et al. (2018), as a result of the hidden Markov structure of the learning problem. Our key innovation lies in algorithmic design. The work of Spantini et al. (2018) adopts a *variational* approach that builds an approximate map by minimizing the statistical divergence of the pushforward of some reference density under the candidate map from the target density. The training procedure of the variational approach is often quite involved—the objective function presents many local

minima and each optimization iteration requires repeated evaluations of the target density at transformed reference variables under the candidate map. In comparison, our algorithmic design utilizes multi-linear function approximation to directly approximate marginal and conditional densities of interest. In addition to the benefit of bypassing nonlinear optimization, we can exploit the TT-based approximations to compute the *exact* KR rearrangement of the *approximate* density in both lower-triangular and upper-triangular forms. This enables us to solve the filtering problem (5) and the smoothing problem (8) using different conditional KR rearrangements constructed from the same approximate density.

In Section 4, we discuss the error accumulation of our proposed algorithms. In Section 5, we present a set of preconditioning techniques for our sequential learning problems to further improve the approximation power of TT. These preconditioning techniques are also given in the form of KR rearrangements. In Section 6, we present a set of numerical experiments to demonstrate the efficacy and efficiency of our proposed methods and compare them to particle-based methods. Our code is accessible online via <https://github.com/DeepTransport/tensor-ssm-paper-demo>.

1.4 Notation

The dimensionalities of the state-space \mathcal{X} , the data space \mathcal{Y} , and the parameter space Θ are m , n , and d , respectively. We assume that the spaces \mathcal{X} , \mathcal{Y} , and Θ can be expressed as Cartesian products. We denote the j -th element of a vector \mathbf{x} by x_j . The index $t \in \mathbb{Z}$ is specifically reserved for denoting the time throughout the paper. For a state random vector \mathbf{X}_t and its realization \mathbf{x}_t at time t , their j -th elements are denoted by $X_{t,j}$ and $x_{t,j}$, respectively. The same convention applies to the data vector \mathbf{Y}_t and its realization \mathbf{y}_t .

For a vector $\mathbf{x}_t \in \mathbb{R}^m$ and an index j , it is convenient to group a subset of elements as follows. The vector $\mathbf{x}_{t,<j} = (x_{t,1}, \dots, x_{t,j-1})$ collects the first $j-1$ elements, and the vector $\mathbf{x}_{t,>j} = (x_{t,j+1}, \dots, x_{t,m})$ collects the last $m-j$ elements. Similarly, we have $\mathbf{x}_{t,\leq j} = (x_{t,1}, \dots, x_{t,j})$, $\mathbf{x}_{t,\geq j} = (x_{t,j}, \dots, x_{t,m})$, and $\mathbf{x}_{t,\leq m} \equiv \mathbf{x}_{t,\geq 0} \equiv \mathbf{x}_t$.

We consider probability measures absolutely continuous with respect to the Lebesgue measure. We denote normalized posterior probability densities in the sequential learning problems by p and its unnormalized version by π . Approximations to these densities are denoted by \hat{p} and $\hat{\pi}$, respectively. The Hellinger distance between random variables with densities p and \hat{p} is defined by

$$D_H(p, \hat{p}) = \left(\frac{1}{2} \int (\sqrt{p(\mathbf{x})} - \sqrt{\hat{p}(\mathbf{x})})^2 d\mathbf{x} \right)^{\frac{1}{2}}.$$

We denote the m -dimensional uniform random variable on a unit hypercube by $\Xi \sim \text{uniform}(\xi; [0, 1]^m)$, in which we drop $[0, 1]^m$ in the definition when no confusion arises.

Consider a diffeomorphism $\mathcal{S}: \mathcal{X} \rightarrow \mathcal{U}$, where $\mathcal{X}, \mathcal{U} \subseteq \mathbb{R}^m$. The density of the transformed variable $\mathcal{S}(\mathbf{X})$ where $\mathbf{X} \sim p$, is the *pushforward* of p under \mathcal{S} , which takes the form

$$\mathcal{S}_\sharp p(\mathbf{u}) = p(\mathcal{S}^{-1}(\mathbf{u})) |\nabla \mathcal{S}^{-1}(\mathbf{u})|.$$

Similarly, the density of the transformed variable $\mathcal{S}^{-1}(\mathbf{U})$ is the *pullback* of the density of \mathbf{U} , denoted by η , under \mathcal{S} , which takes the form

$$\mathcal{S}^\sharp \eta(\mathbf{x}) = \eta(\mathcal{S}(\mathbf{x})) |\nabla \mathcal{S}(\mathbf{x})|.$$

Here $|\cdot|$ denotes the determinant of a matrix.

2 TT-based recursive posterior approximation

We first discuss the recursive formula outlining the design principle of sequential learning problems. We then introduce TT decomposition and present a basic implementation of the TT-based sequential learning algorithm.

2.1 Recursive state and parameter learning

Following the definition of the joint density of $(\boldsymbol{\Theta}, \mathbf{X}_{0:t}, \mathbf{Y}_{1:t})$ in (3), the density of the posterior random variables $(\boldsymbol{\Theta}, \mathbf{X}_{0:t} | \mathbf{Y}_{1:t} = \mathbf{y}_{1:t})$ also has a recursive form

$$p(\boldsymbol{\theta}, \mathbf{x}_{0:t} | \mathbf{y}_{1:t}) = \frac{p(\boldsymbol{\theta}, \mathbf{x}_{0:t-1} | \mathbf{y}_{1:t-1}) f(\mathbf{x}_t | \mathbf{x}_{t-1}, \boldsymbol{\theta}) g(\mathbf{y}_t | \mathbf{x}_t, \boldsymbol{\theta})}{p(\mathbf{y}_t | \mathbf{y}_{1:t-1})}, \quad (9)$$

where $p(\mathbf{y}_t | \mathbf{y}_{1:t-1})$ is a computationally intractable conditional evidence. Marginalizing both sides over $\mathbf{X}_{0:t-2}$, the parameter $\boldsymbol{\Theta}$ and adjacent states $(\mathbf{X}_t, \mathbf{X}_{t-1})$ jointly follow the posterior density

$$p(\boldsymbol{\theta}, \mathbf{x}_t, \mathbf{x}_{t-1} | \mathbf{y}_{1:t}) = \frac{p(\boldsymbol{\theta}, \mathbf{x}_{t-1} | \mathbf{y}_{1:t-1}) f(\mathbf{x}_t | \mathbf{x}_{t-1}, \boldsymbol{\theta}) g(\mathbf{y}_t | \mathbf{x}_t, \boldsymbol{\theta})}{p(\mathbf{y}_t | \mathbf{y}_{1:t-1})}. \quad (10)$$

The above formula outlines basic steps needed by a sequential estimation algorithm to solve the filtering problem (5) and the parameter estimation problem (6):

1. At time $t-1$, the posterior random variables $(\boldsymbol{\Theta}, \mathbf{X}_{t-1} | \mathbf{Y}_{1:t-1} = \mathbf{y}_{1:t-1})$ has the density $p(\boldsymbol{\theta}, \mathbf{x}_{t-1} | \mathbf{y}_{1:t-1})$.
2. At time t , using the state transition density $f(\mathbf{x}_t | \mathbf{x}_{t-1}, \boldsymbol{\theta})$ and the likelihood function $g(\mathbf{y}_t | \mathbf{x}_t, \boldsymbol{\theta})$, we can compute the joint posterior density $p(\boldsymbol{\theta}, \mathbf{x}_t, \mathbf{x}_{t-1} | \mathbf{y}_{1:t})$, up to the unknown evidence $p(\mathbf{y}_t | \mathbf{y}_{1:t-1})$.
3. We obtain the density for the new posterior random variables $(\boldsymbol{\Theta}, \mathbf{X}_t | \mathbf{Y}_{1:t} = \mathbf{y}_{1:t})$ by solving a marginalization problem

$$p(\boldsymbol{\theta}, \mathbf{x}_t | \mathbf{y}_{1:t}) = \int_{\mathcal{X}} p(\boldsymbol{\theta}, \mathbf{x}_t, \mathbf{x}_{t-1} | \mathbf{y}_{1:t}) d\mathbf{x}_{t-1}. \quad (11)$$

In these steps, the marginalization in (11) plays the key role in sequentially updating the joint posterior random variables $(\boldsymbol{\Theta}, \mathbf{X}_t | \mathbf{Y}_{1:t} = \mathbf{y}_{1:t})$. For example, the bootstrap filter (Gordon et al., 1993) solves the marginalization by a weighted update of conditional samples—it first draws conditional random variables $\mathbf{X}_t^{(i)} | \mathbf{X}_{t-1}^{(i)}$ that follow the state transition density $f(\mathbf{x}_t | \mathbf{X}_{t-1}^{(i)})$ conditioned on each of the previous particles, and then updates the weights using the likelihood function $g(\mathbf{y}_t | \mathbf{X}_t^{(i)})$. The path estimation (7) and the smoothing (8) can be solved by additional backpropagation steps given the solutions to the filtering and parameter estimation problems. In the rest of this section, we will introduce the TT decomposition that can solve the marginalization problem (11) by function approximation, and then present a basic TT-based algorithm to outline the procedure for solving the filtering and parameter estimation problems. Algorithms for solving the smoothing problem will be discussed in later sections.

2.2 TT decomposition

The central computational tool used in this work is the functional TT decomposition (Bigoni et al., 2016; Gorodetsky et al., 2019). Consider we have a general multivariate function $f : \mathcal{X} \rightarrow \mathbb{R}$ where $\mathcal{X} \in \mathbb{R}^m$ is a Cartesian product. Then, one can approximately decompose $h(\mathbf{x})$ in the following form

$$h(\mathbf{x}) \approx \hat{h}(\mathbf{x}) = \sum_{\alpha_0=1}^{r_0} \sum_{\alpha_1=1}^{r_1} \cdots \sum_{\alpha_m=1}^{r_m} \mathsf{H}_1^{(\alpha_0, \alpha_1)}(x_1) \cdots \mathsf{H}_k^{(\alpha_{k-1}, \alpha_k)}(x_k) \cdots \mathsf{H}_m^{(\alpha_{m-1}, \alpha_m)}(x_m),$$

where $r_0 = r_m = 1$ and the summation ranges r_0, r_1, \dots, r_m are called TT ranks. Each scalar-valued univariate function $\mathsf{H}_k^{(\alpha_{k-1}, \alpha_k)}(x_k)$ is represented as a linear combination of a set of ℓ_k basis functions $\{\phi_k^{(1)}(x_k), \dots, \phi_k^{(\ell_k)}(x_k)\}$, which yields

$$\mathsf{H}_k^{(\alpha_{k-1}, \alpha_k)}(x_k) = \sum_{j=1}^{\ell_k} \phi_k^{(j)}(x_k) \mathbf{A}_k[\alpha_{k-1}, j, \alpha_k],$$

where $\mathbf{A}_k \in \mathbb{R}^{r_{k-1} \times \ell_k \times r_k}$ is an order-3 coefficient tensor. Examples of the basis functions include piecewise polynomials, orthogonal functions, radial basis functions, etc. Grouping all scalar-valued univariate functions $\mathsf{H}_k^{(\alpha_{k-1}, \alpha_k)}(x_k)$ for each coordinate x_k yields a matrix-valued function $\mathsf{H}_k(x_k) : \mathcal{X}_k \rightarrow \mathbb{R}^{r_{k-1} \times r_k}$, which is referred to as the k -th tensor core. This way, the decomposed function can also be expressed as a sequence of multiplications of matrix-valued univariate functions, which is given by

$$\hat{h}(\mathbf{x}) = \mathsf{H}_1(x_1) \cdots \mathsf{H}_k(x_k) \cdots \mathsf{H}_m(x_m). \quad (12)$$

The TT decomposition can be computed efficiently for a wide range of densities via alternating linear schemes together with cross approximation (Bigoni et al., 2016; Gorodetsky et al., 2019; Oseledets and Tyrtyshnikov, 2010). We employ the functional extension of the alternating minimal energy method with a residual-based rank adaptation of (Dolgov and Savostyanov, 2014). It requires only $\mathcal{O}(mlr^2)$ evaluations of the function f and $\mathcal{O}(mlr^3)$ floating point operations, where $\ell = \max_k \ell_k$ and $r = \max_k r_k$. In general, the maximal rank r depends on the dimension m and can be large when the function f concentrates in some part of its domain. Some theoretical results exist that provide rank bounds. For example, the work of Rohrbach et al. (2022) establishes specific bounds for certain multivariate Gaussian densities that depend poly-logarithmically on m , while the work of Griebel and Harbrecht (2023) proves dimension-independent bounds for general functions in weighted spaces with dominating mixed smoothness.

The integration of the factorized function \hat{h} can be simplified to integral of certain univariate tensor cores. For example, the integral over x_k can be calculated as

$$\begin{aligned} \int \hat{h}(x_1, x_2, \dots, x_m) dx_k &= \int \mathsf{H}_1(x_k) \cdots \mathsf{H}_k(x_k) \cdots \mathsf{H}_m(x_m) dx_k \\ &= \overline{\mathsf{H}}_k(x_1) \cdots \overline{\mathsf{H}}_k \cdots \mathsf{H}_1(x_m), \end{aligned} \quad (13)$$

where the overlined matrix $\overline{\mathsf{H}}_k = \int \mathsf{H}_k(x_k) dx_k \in \mathbb{R}^{r_{k-1} \times r_k}$ is obtained by integrating the k -th tensor core. This way, the cost of the integration problem scales linearly in the number of variables and quadratically in tensor ranks. This opens the door to solving the marginalization step in sequential learning problems.

2.3 Basic algorithm

We integrate the TT decomposition and the recursive formula in Section 2.1 to design a basic TT-based algorithm for solving the sequential learning problems. Although this basic algorithm does not require a particular variable ordering, we order the variables as $(\mathbf{x}_t, \boldsymbol{\theta}, \mathbf{x}_{t-1})$ to be compatible with algorithms that will be introduced in Section 3.2.

At time $t-1$, suppose the density of the posterior variables $(\boldsymbol{\Theta}, \mathbf{X}_{t-1} | \mathbf{Y}_{1:t-1} = \mathbf{y}_{1:t-1})$ is approximated by a TT decomposition, i.e.,

$$p(\boldsymbol{\theta}, \mathbf{x}_{t-1} | \mathbf{y}_{1:t-1}) \propto \hat{\pi}(\boldsymbol{\theta}, \mathbf{x}_{t-1} | \mathbf{y}_{1:t-1}),$$

where $a \propto b$ denotes that a is approximately proportional to b . Then, for new observed data \mathbf{y}_t , we can recursively approximate the new density of the joint posterior random variables $(\boldsymbol{\Theta}, \mathbf{X}_t | \mathbf{Y}_{1:t} = \mathbf{y}_{1:t})$, the filtering density of $(\mathbf{X}_t | \mathbf{Y}_{1:t} = \mathbf{y}_{1:t})$ and the posterior parameter density $(\boldsymbol{\Theta} | \mathbf{Y}_{1:t} = \mathbf{y}_{1:t})$ as follows.

Algorithm 1: TT-based sequential estimation.

(a) **Non-separable approximation.** Following (10), the density of the joint posterior random variables $(\mathbf{X}_t, \boldsymbol{\Theta}, \mathbf{X}_{t-1} | \mathbf{Y}_{1:t} = \mathbf{y}_{1:t})$ yields a non-separable, unnormalized approximation q_t in the form of

$$q_t(\mathbf{x}_t, \boldsymbol{\theta}, \mathbf{x}_{t-1}) := \hat{\pi}(\mathbf{x}_{t-1}, \boldsymbol{\theta} | \mathbf{y}_{1:t-1}) f(\mathbf{x}_t | \mathbf{x}_{t-1}, \boldsymbol{\theta}) g(\mathbf{y}_t | \mathbf{x}_t, \boldsymbol{\theta}), \quad (14)$$

which can be evaluated pointwise.

(b) **Separable approximation.** We re-approximate the non-separable unnormalized density q_t by a TT decomposition $\hat{\pi}$, i.e.,

$$\begin{aligned} q_t(\mathbf{x}_t, \boldsymbol{\theta}, \mathbf{x}_{t-1}) &\approx \hat{\pi}(\mathbf{x}_t, \boldsymbol{\theta}, \mathbf{x}_{t-1} | \mathbf{y}_{1:t}) \\ &= \mathsf{F}_1(x_{t,1}) \cdots \mathsf{F}_m(x_{t,m}) \mathsf{G}_1(\theta_1) \cdots \mathsf{G}_d(\theta_d) \mathsf{H}_1(x_{t-1,1}) \cdots \mathsf{H}_m(x_{t-1,m}), \end{aligned}$$

where F , G and H denote tensor cores for the state at time t , the parameters, and the state at time $t-1$, respectively.

(c) **Integration.** By integrating the TT-approximation $\hat{\pi}$, we are able to approximate the density for the posterior random variables $(\boldsymbol{\Theta}, \mathbf{X}_t | \mathbf{Y}_{1:t} = \mathbf{y}_{1:t})$ by

$$\begin{aligned} \hat{\pi}(\mathbf{x}_t, \boldsymbol{\theta} | \mathbf{y}_{1:t}) &= \int \hat{\pi}(\mathbf{x}_t, \boldsymbol{\theta}, \mathbf{x}_{t-1} | \mathbf{y}_{1:t}) d\mathbf{x}_{t-1} \\ &= \mathsf{F}_1(x_{t,1}) \cdots \mathsf{F}_m(x_{t,m}) \mathsf{G}_1(\theta_1) \cdots \mathsf{G}_d(\theta_d) (\bar{\mathsf{H}}_1 \cdots \bar{\mathsf{H}}_m), \end{aligned}$$

and the normalizing constant

$$c_t = \int \hat{\pi}(\mathbf{x}_t, \boldsymbol{\theta}, \mathbf{x}_{t-1} | \mathbf{y}_{1:t}) d\mathbf{x}_t d\boldsymbol{\theta} d\mathbf{x}_{t-1} = \bar{\mathsf{F}}_1 \cdots \bar{\mathsf{F}}_m \bar{\mathsf{G}}_1 \cdots \bar{\mathsf{G}}_d \bar{\mathsf{H}}_1 \cdots \bar{\mathsf{H}}_m.$$

The densities of the posterior parameter $(\boldsymbol{\Theta} | \mathbf{Y}_{1:t} = \mathbf{y}_{1:t})$ and the filtering state $(\mathbf{X}_t | \mathbf{Y}_{1:t} = \mathbf{y}_{1:t})$ can be approximated in a similar way.

In the next step $t + 1$, we can apply the same procedure using the newly computed approximation $\hat{\pi}(\mathbf{x}_t, \boldsymbol{\theta} | \mathbf{y}_{1:t})$.

The above basic TT-based algorithm reveals some of the key principles of the algorithms introduced in this paper. Given the existing approximation $\hat{\pi}(\mathbf{x}_{t-1}, \boldsymbol{\theta} | \mathbf{y}_{1:t-1})$, the joint posterior random variables $(\mathbf{X}_t, \boldsymbol{\Theta}, \mathbf{X}_{t-1} | \mathbf{Y}_{1:t} = \mathbf{y}_{1:t})$ yield a non-separable, unnormalized approximate density q_t in step (a) of Alg. 1. Since q_t cannot be directly marginalized, we re-approximate q_t using a new TT in step (b) of Alg. 1, which enables further marginalizations in step (c) of Alg. 1.

In Sections 3 and 4, we design new algorithms to remove estimation biases due to approximation errors, and analyze the accumulation of approximation errors over time. However, the rank truncation used by TT may not preserve the non-negativity of density functions. An analogue is that the truncated singular value decomposition of a non-negative matrix may contain negative entries. The non-negativity is essential for designing transport maps for debiasing. We will overcome this barrier by using an alternative form of TT decomposition. Since the complexity and approximation power of TT-based algorithms crucially relies on the tensor ranks, we develop preconditioning methods in Section 5 to improve the efficiency of our proposed algorithms.

3 Squared-TT algorithms, debiasing and smoothing

We first review the squared-TT method for building KR rearrangements, which is originally introduced in Cui and Dolgov (2022). We then integrate the resulting transport maps into the recursive procedure defined in Section 2.3 to sequentially solve the filtering problem (5) and the parameter estimation problem (6) with sample-based debiasing. We also design an algorithm to solve the smoothing problem (8) with additional backpropagation steps.

3.1 Squared TT and KR rearrangement

Consider the normalized target probability density $p(\mathbf{x}) = \frac{1}{z}\pi(\mathbf{x})$ with $\mathbf{x} \in \mathbb{R}^m$, in which z is an unknown constant and we can only evaluate the unnormalized density $\pi(\mathbf{x})$. To preserve non-negativity in function approximation, one can decompose the square root of $\pi(\mathbf{x})$, i.e.,

$$\sqrt{\pi(\mathbf{x})} \approx \phi(\mathbf{x}) = \mathbf{H}_1(x_1) \cdots \mathbf{H}_m(x_m).$$

Then, the approximate density function $\phi(\mathbf{x})^2$ is non-negative for all \mathbf{x} by construction. Given some reference tensor-product probability density $\lambda(\mathbf{x}) := \prod_{i=1}^m \lambda_i(x_i)$ such that $\sup_{\mathbf{x}} \pi(\mathbf{x})/\lambda(\mathbf{x}) < \infty$ and a sufficiently small constant $\tau > 0$, we can further construct a defensive version of the approximate density function

$$\hat{p}(\mathbf{x}) = \frac{1}{\hat{z}}\hat{\pi}(\mathbf{x}), \quad \hat{\pi}(\mathbf{x}) = \phi(\mathbf{x})^2 + \tau\lambda(\mathbf{x}), \quad \hat{z} = \int \hat{\pi}(\mathbf{x}) d\mathbf{x}. \quad (15)$$

The approximate density \hat{p} satisfies $\sup_{\mathbf{x}} p(\mathbf{x})/\hat{p}(\mathbf{x}) < \infty$, which is essential to ensure that importance sampling estimators defined by \hat{p} satisfy the central limit theorem. Based on mild assumptions, the following lemma establishes the L^2 error of $\sqrt{\hat{\pi}}$ and the Hellinger error of the normalized approximation \hat{p} .

Lemma 1 Suppose the TT approximation ϕ satisfies $\|\phi - \sqrt{\pi}\|_{L^2} \leq \epsilon$ and the constant τ satisfies $\tau \leq \|\phi - \sqrt{\pi}\|_{L^2}^2$. Then, the L^2 error of $\sqrt{\hat{\pi}}$ defined in (15) satisfies $\|\sqrt{\hat{\pi}} - \sqrt{\pi}\|_{L^2} \leq \sqrt{2\epsilon}$. The Hellinger distance between p and its normalized approximation \hat{p} defined in (15) satisfies

$$D_H(\hat{p}, p) \leq \frac{\sqrt{2}}{\sqrt{z}} \|\sqrt{\hat{\pi}} - \sqrt{\pi}\|_{L^2} \leq \frac{2\epsilon}{\sqrt{z}}.$$

Proof The bounds on the L^2 and Hellinger errors are shown in Proposition 4 and Theorem 1 of Cui and Dolgov (2022), respectively. \blacksquare

As outlined in Section 2.3, marginalization of the approximation is a key operation in deriving the recursive algorithm. For the squared TT approximation defined in (15), the following (Cui and Dolgov, 2022, Proposition 2) gives its marginal density.

Proposition 2 We consider the normalized approximation \hat{p} defined in (15). For the TT decomposition $\phi(\mathbf{x}) = \mathbf{H}_1(x_1) \cdots \mathbf{H}_m(x_m)$ and a given index $1 \leq k < m$, we define the left accumulated tensor core as $\mathbf{H}_{\leq k}(\mathbf{x}_{\leq k}) = \mathbf{H}_1(x_1) \cdots \mathbf{H}_k(x_k) \in \mathbb{R}^{1 \times r_k}$ and the right accumulated tensor core as $\mathbf{H}_{>k}(\mathbf{x}_{>k}) = \mathbf{H}_{k+1}(x_{k+1}) \cdots \mathbf{H}_m(x_m) \in \mathbb{R}^{r_k \times 1}$. Then the marginal density of \hat{p} takes the form

$$\hat{p}(\mathbf{x}_{\leq k}) = \int \hat{p}(\mathbf{x}) d\mathbf{x}_{>k} = \frac{1}{\hat{z}} \left(\sum_{\gamma_k=1}^{r_k} \left(\sum_{\alpha_k=1}^{r_k} \mathbf{H}_{\leq k}^{(\alpha_k)}(\mathbf{x}_{\leq k}) \mathbf{L}_{>k}^{(\alpha_k, \gamma_k)} \right)^2 + \tau \lambda(\mathbf{x}_{\leq k}) \right), \quad (16)$$

where $\lambda(\mathbf{x}_{\leq k}) = \prod_{i=1}^k \lambda_i(x_i)$ and $\mathbf{L}_{>k} \in \mathbb{R}^{r_k \times r_k}$ is the (lower-triangular) Cholesky decomposition of the accumulated mass matrix

$$\mathbf{M}_{>k}^{(\alpha_k, \beta_k)} = \int \mathbf{H}_{>k}^{(\alpha_k)}(\mathbf{x}_{>k}) \mathbf{H}_{>k}^{(\beta_k)}(\mathbf{x}_{>k}) d\mathbf{x}_{>k}, \quad \alpha_k = 1, \dots, r_k, \quad \beta_k = 1, \dots, r_k.$$

As shown in Cui and Dolgov (2022), the Cholesky decomposition in Proposition 2 can be recursively computed from $k = m - 1$ to $k = 1$. The normalizing constant \hat{z} can also be computed in a similar way as the last iteration of the recursion. Computing all marginal densities $\hat{p}(x_1), \dots, \hat{p}(x_{\leq m-1})$ requires $\mathcal{O}(m\ell r^3)$ floating point operations.

The normalized approximate density \hat{p} defines a new random variable $\hat{\mathbf{X}}$. Using the marginal densities constructed in Proposition 2, the densities of random variables $\hat{X}_1, \hat{X}_2 | \hat{X}_1, \dots, \hat{X}_k | \hat{\mathbf{X}}_{<k}, \dots, \hat{X}_m | \hat{\mathbf{X}}_{<m}$ are given by $\hat{p}(x_1)$ and

$$\hat{p}(x_k | \mathbf{x}_{<k}) = \frac{\hat{p}(\mathbf{x}_{\leq k})}{\hat{p}(\mathbf{x}_{<k})} = \frac{\phi(\mathbf{x}_{\leq k})^2 + \tau \lambda(\mathbf{x}_{\leq k})}{\phi(\mathbf{x}_{<k})^2 + \tau \lambda(\mathbf{x}_{<k})}, \quad k = 2, 3, \dots, m,$$

respectively. The corresponding distribution functions

$$F_1(x_1) = \int_{-\infty}^{x_1} \hat{p}(x'_1) dx'_1 \quad \text{and} \quad F_k(x_k | \mathbf{x}_{<k}) = \int_{-\infty}^{x_k} \hat{p}(x'_k | \mathbf{x}_{<k}) dx'_k \quad (17)$$

defines an order-preserving map $\mathcal{F} : \mathbb{R}^m \mapsto [0, 1]^m$ in the form of

$$\mathcal{F}(\mathbf{x}) = [F_1(x_1), \dots, F_k(x_k | \mathbf{x}_{<k}), \dots, F_m(x_m | \mathbf{x}_{<m})]^\top, \quad (18)$$

which is commonly referred to as the KR rearrangement (Rosenblatt, 1952; Knothe et al., 1957). The map \mathcal{F} transforms a random variable $\tilde{\mathbf{X}} \sim \hat{p}(\mathbf{x})$ into a uniform random variable $\Xi \sim \text{uniform}(\xi)$, i.e., $\Xi = \mathcal{F}(\mathbf{X})$. Since the k -th component of \mathcal{F} depends on only the previous $k-1$ coordinates, both \mathcal{F} and its inverse \mathcal{F}^{-1} have triangular structures, and thus can be evaluated dimension-by-dimension.

The complexities of evaluating \mathcal{F} and \mathcal{F}^{-1} are dominated by the dimension-by-dimension evaluation of the conditional densities $\hat{p}(x_k | \mathbf{x}_{<k})$, $k = 2, \dots, m$ and the corresponding distribution functions, which is $\mathcal{O}(mlr^2)$ in total. Evaluating the above defined KR rearrangement is less computationally costly than building the marginal densities.

Remark 3 Note the marginal density $\hat{p}(\mathbf{x}_{\geq k})$, $k = 2, \dots, m$ can be computed in a similar way from the first coordinate to the last coordinate. In this way, the resulting KR rearrangement is upper-triangular, i.e.,

$$\mathcal{F}^u(\mathbf{x}) = [F_1(x_1 | \mathbf{x}_{>1}), \dots, F_k(x_k | \mathbf{x}_{>k}), \dots, F_m(x_m)]^\top, \quad (19)$$

as the variable dependency follows a reverse order.

3.2 Non-negativity-preserving algorithm and conditional maps

Following the steps of the basic algorithm (cf. Alg. 1), we first define a new sequential learning algorithm using the non-negativity-preserving approximation presented in (15), and then construct the associated conditional KR rearrangements. The conditional KR rearrangements will be used to sequentially generate weighted samples to correct for approximation bias.

Algorithm 2: Sequential estimation using squared-TT approximations.

(a) **Non-separable approximation.** At time $t-1$, suppose the posterior random variables $(\boldsymbol{\Theta}, \mathbf{X}_{t-1} | \mathbf{Y}_{1:t-1})$ has a TT-based (unnormalized) approximate density $\hat{\pi}(\boldsymbol{\theta}, \mathbf{x}_{t-1} | \mathbf{y}_{1:t-1})$. The density of the new joint posterior random variables $(\mathbf{X}_t, \boldsymbol{\Theta}, \mathbf{X}_{t-1} | \mathbf{Y}_{1:t} = \mathbf{y}_{1:t})$ yields a non-separable, unnormalized approximation

$$q_t(\mathbf{x}_t, \boldsymbol{\theta}, \mathbf{x}_{t-1}) := \hat{\pi}(\mathbf{x}_{t-1}, \boldsymbol{\theta} | \mathbf{y}_{1:t-1}) f(\mathbf{x}_t | \mathbf{x}_{t-1}, \boldsymbol{\theta}) g(\mathbf{y}_t | \mathbf{x}_t, \boldsymbol{\theta}). \quad (20)$$

(b) **Separable approximation.** We re-approximate the square root of q_t by a TT decomposition ϕ_t , i.e.,

$$\begin{aligned} \sqrt{q_t(\mathbf{x}_t, \boldsymbol{\theta}, \mathbf{x}_{t-1})} &\approx \phi_t(\mathbf{x}_t, \boldsymbol{\theta}, \mathbf{x}_{t-1}) \\ &= \mathsf{G}_1(x_{t,1}) \cdots \mathsf{G}_m(x_{t,m}) \mathsf{F}_1(\theta_1) \cdots \mathsf{F}_d(\theta_d) \mathsf{H}_1(x_{t-1,1}) \cdots \mathsf{H}_m(x_{t-1,m}). \end{aligned} \quad (21)$$

and choose a constant τ_t such that $\tau_t \leq \|\phi_t - \sqrt{q_t}\|_{L^2}^2$. Following the construction in (15), this gives a non-negative approximation

$$\hat{\pi}(\mathbf{x}_t, \boldsymbol{\theta}, \mathbf{x}_{t-1} | \mathbf{y}_{1:t}) = \phi_t(\mathbf{x}_t, \boldsymbol{\theta}, \mathbf{x}_{t-1})^2 + \tau_t \lambda(\mathbf{x}_t) \lambda(\boldsymbol{\theta}) \lambda(\mathbf{x}_{t-1}). \quad (22)$$

(c) **Integration.** Applying Proposition 2 from the right variable $x_{t-1,m}$ to the left variable $x_{t-1,1}$, we obtain $\hat{\pi}(\mathbf{x}_t, \boldsymbol{\theta} | \mathbf{y}_{1:t}) = \int \hat{\pi}(\mathbf{x}_t, \boldsymbol{\theta}, \mathbf{x}_{t-1} | \mathbf{y}_{1:t}) d\mathbf{x}_{t-1}$.

In the next step $t+1$, we can apply the same procedure using the newly computed marginal approximation $\hat{\pi}(\mathbf{x}_t, \boldsymbol{\theta} | \mathbf{y}_{1:t})$.

Using Proposition 2, we can integrate the approximate density $\hat{\pi}(\mathbf{x}_t, \boldsymbol{\theta}, \mathbf{x}_{t-1} | \mathbf{y}_{1:t})$ from the right variable $x_{t-1,m}$ to the left variable $x_{t,1}$ to define the lower-triangular KR rearrangement $\mathcal{F}_t^l : \mathcal{X} \times \Theta \times \mathcal{X} \rightarrow [0, 1]^{2m+d}$ in the form of

$$\mathcal{F}_t^l(\mathbf{x}_t, \boldsymbol{\theta}, \mathbf{x}_{t-1}) = \begin{bmatrix} \mathcal{F}_{t,t}^l(\mathbf{x}_t) \\ \mathcal{F}_{t,\theta}^l(\boldsymbol{\theta} | \mathbf{x}_t) \\ \mathcal{F}_{t,t-1}^l(\mathbf{x}_{t-1} | \mathbf{x}_t, \boldsymbol{\theta}) \end{bmatrix} = \begin{bmatrix} F_{t,t,1}(x_{t,1}) \\ \vdots \\ F_{t,t,m}(x_{t,m} | \mathbf{x}_{t,<m}) \\ \vdots \\ F_{t,\theta,k}(\theta_k | \mathbf{x}_t, \boldsymbol{\theta}_{<k}) \\ \vdots \\ F_{t,t-1,1}(x_{t-1,1} | \mathbf{x}_t, \boldsymbol{\theta}) \\ \vdots \\ F_{t,t-1,m}(x_{t-1,m} | \mathbf{x}_t, \boldsymbol{\theta}, \mathbf{x}_{t-1,<m}) \end{bmatrix}, \quad (23)$$

in which each scalar-valued function $F_{t,\cdot,\cdot}$ is a (conditional) distribution function. For example, we have

$$F_{t,t-1,k}(x_{t-1,k} | \mathbf{x}_t, \boldsymbol{\theta}, \mathbf{x}_{t-1,<k}) = \int_{-\infty}^{x_{t-1,k}} \frac{\hat{\pi}(\mathbf{x}_t, \boldsymbol{\theta}, \mathbf{x}_{t-1,<k}, x'_{t-1,k} | \mathbf{y}_{1:t})}{\hat{\pi}(\mathbf{x}_t, \boldsymbol{\theta}, \mathbf{x}_{t-1,<k} | \mathbf{y}_{1:t})} dx'_{t-1,k}. \quad (24)$$

The inverse map $(\mathcal{F}_t^l)^{-1}$ transforms uniform random variables to the approximate posterior random variables $(\hat{\mathbf{X}}_t, \hat{\boldsymbol{\Theta}}, \hat{\mathbf{X}}_{t-1} | \mathbf{Y}_{1:t} = \mathbf{y}_{1:t}) \sim \hat{p}$, where $\hat{p}(\mathbf{x}_t, \boldsymbol{\theta}, \mathbf{x}_{t-1} | \mathbf{y}_{1:t}) \propto \hat{\pi}(\mathbf{x}_t, \boldsymbol{\theta}, \mathbf{x}_{t-1} | \mathbf{y}_{1:t})$.

Note that the construction of conditional distribution functions—for example, (24)—does not require the normalizing constant of the approximate density $\hat{\pi}$, because the marginal densities share the same normalizing constant. Thus, by only integrating the state \mathbf{x}_{t-1} dimension-by-dimension from the right variable $x_{t-1,m}$ to the left variable $x_{t-1,1}$, we obtain the lower conditional KR rearrangement

$$\mathcal{F}_{t,t-1}^l(\mathbf{x}_{t-1} | \mathbf{x}_t, \boldsymbol{\theta}) = \begin{bmatrix} F_{t,t-1,1}(x_{t-1,1} | \mathbf{x}_t, \boldsymbol{\theta}) \\ \vdots \\ F_{t,t-1,m}(x_{t-1,m} | \mathbf{x}_t, \boldsymbol{\theta}, \mathbf{x}_{t-1,<m}) \end{bmatrix}. \quad (25)$$

The following proposition shows that the lower conditional map $\mathcal{F}_{t,t-1}^l$ defines a *backward* sampler, which generates samples backward in time from the conditional density $\hat{p}(\mathbf{x}_{t-1} | \mathbf{x}_t, \boldsymbol{\theta}, \mathbf{y}_{1:t})$. This is particularly useful for defining smoothing algorithms.

Proposition 4 *Conditioned on $\hat{\mathbf{X}}_t = \mathbf{x}_t, \hat{\boldsymbol{\Theta}} = \boldsymbol{\theta}$, inverting the lower conditional KR rearrangement $\mathcal{F}_{t,t-1}^l$ defined in (25), we are able to transform a uniform random variable to the conditional random variable*

$$(\hat{\mathbf{X}}_{t-1} | \hat{\mathbf{X}}_t = \mathbf{x}_t, \hat{\boldsymbol{\Theta}} = \boldsymbol{\theta}, \mathbf{Y}_{1:t} = \mathbf{y}_{1:t}) \sim \hat{p}(\mathbf{x}_{t-1} | \mathbf{x}_t, \boldsymbol{\theta}, \mathbf{y}_{1:t}).$$

Proof Conditioned on $\hat{\mathbf{X}}_t = \mathbf{x}_t, \hat{\boldsymbol{\Theta}} = \boldsymbol{\theta}$, the Jacobian of $\mathcal{F}_{t,t-1}^l(\cdot | \mathbf{x}_t, \boldsymbol{\theta})$, denoted by $\mathbf{J} \in \mathbb{R}^{m \times m}$, is an lower triangular matrix with diagonal entries

$$J_{kk} = \frac{\partial F_{t,t-1,k}(x_{t-1,k} | \mathbf{x}_t, \boldsymbol{\theta}, \mathbf{x}_{t-1,<k})}{\partial x_{t-1,k}} = \hat{p}(x_{t-1,k} | \mathbf{x}_t, \boldsymbol{\theta}, \mathbf{x}_{t-1,<k}, \mathbf{y}_{1:t}), \quad k = 1, \dots, m,$$

by (24). Thus, the pullback of the uniform density under $\mathcal{F}_{t,t-1}^l(\cdot|\mathbf{x}_t, \boldsymbol{\theta})$ is

$$(\mathcal{F}_{t,t-1}^l)^\sharp \text{uniform}(\mathbf{x}_t) = |\mathbf{J}| = \prod_{k=1}^m \hat{p}(x_{t-1,k}|\mathbf{x}_t, \boldsymbol{\theta}, \mathbf{x}_{t-1,<k}, \mathbf{y}_{1:t}) = \hat{p}(x_{t-1}|\mathbf{x}_t, \boldsymbol{\theta}, \mathbf{y}_{1:t}).$$

This concludes the result. \blacksquare

Similarly, one can integrate the state \mathbf{x}_t in the approximation $\hat{\pi}(\mathbf{x}_t, \boldsymbol{\theta}, \mathbf{x}_{t-1}|\mathbf{y}_{1:t})$ from the left variable $x_{t,1}$ to the right variable $x_{t,m}$ to define an upper conditional KR rearrangement

$$\mathcal{F}_{t,t}^u(\mathbf{x}_t|\boldsymbol{\theta}, \mathbf{x}_{t-1}) = \begin{bmatrix} F_{t,t,1}(x_{t,1}|\mathbf{x}_{t,>1}, \boldsymbol{\theta}, \mathbf{x}_{t-1}) \\ \vdots \\ F_{t,t,m}(x_{t,m}|\boldsymbol{\theta}, \mathbf{x}_{t-1}) \end{bmatrix}, \quad (26)$$

Inverting the conditional map $\mathcal{F}_{t,t}^u$, we are able to transform a uniform random variable to the conditional random variable

$$(\hat{\mathbf{X}}_t|\hat{\boldsymbol{\Theta}} = \boldsymbol{\theta}, \hat{\mathbf{X}}_{t-1} = \mathbf{x}_{t-1}, \mathbf{Y}_{1:t} = \mathbf{y}_{1:t}) \sim \hat{p}(\mathbf{x}_t|\boldsymbol{\theta}, \mathbf{x}_{t-1}, \mathbf{y}_{1:t}).$$

This way, the upper conditional map $\mathcal{F}_{t,t}^u$ defines a *forward* sampler that generates samples forward in time. This will be used in particle filtering.

3.3 Particle filter

The upper conditional map $\mathcal{F}_{t,t}^u$ in (26) naturally define a particle filter accompanying the recursive approximations in Alg. 2. Suppose weighted samples $\{\hat{\boldsymbol{\Theta}}^{(i)}, \hat{\mathbf{X}}_{0:t-1}^{(i)}, W_{t-1}^{(i)}\}_{i=1}^N$ follow the joint posterior density $p(\boldsymbol{\theta}, \mathbf{x}_{0:t-1}|\mathbf{y}_{1:t-1})$ at time $t-1$. Then conditioned on each pair of $\{\hat{\boldsymbol{\Theta}}^{(i)}, \hat{\mathbf{X}}_{t-1}^{(i)}\}_{i=1}^N$, we can invert $\mathcal{F}_{t,t}^u$ to obtain a new sample

$$\hat{\mathbf{X}}_t^{(i)} = (\mathcal{F}_{t,t}^u)^{-1}(\boldsymbol{\Xi}^{(i)}|\hat{\boldsymbol{\Theta}}^{(i)}, \hat{\mathbf{X}}_{t-1}^{(i)}), \quad \boldsymbol{\Xi}^{(i)} \sim \text{uniform}(\boldsymbol{\xi}). \quad (27)$$

The sample $\hat{\mathbf{X}}_t^{(i)}$ follows the conditional density $\hat{p}(\mathbf{x}_t|\boldsymbol{\theta}, \mathbf{x}_{t-1}, \mathbf{y}_{1:t})$. Expanding the sample state path $\hat{\mathbf{X}}_{0:t-1}^{(i)}$ by $\hat{\mathbf{X}}_t^{(i)}$, the updated weighted samples $\{\hat{\boldsymbol{\Theta}}^{(i)}, \hat{\mathbf{X}}_{0:t}^{(i)}, W_{t-1}^{(i)}\}_{i=1}^N$ jointly follow the normalized density

$$\hat{p}(\mathbf{x}_t|\boldsymbol{\theta}, \mathbf{x}_{t-1}, \mathbf{y}_{1:t}) p(\boldsymbol{\theta}, \mathbf{x}_{0:t-1}|\mathbf{y}_{1:t-1}). \quad (28)$$

After applying the sampling procedure in (27), we can update the weights of the updated samples $\{\hat{\boldsymbol{\Theta}}^{(i)}, \hat{\mathbf{X}}_{0:t}^{(i)}, W_{t-1}^{(i)}\}_{i=1}^N$ according to the ratio of the new joint posterior density $p(\boldsymbol{\theta}, \mathbf{x}_{0:t}|\mathbf{y}_{1:t})$ in (9) to the sampling density in (28), i.e.,

$$r_f(\boldsymbol{\theta}, \mathbf{x}_{0:t}) = \frac{p(\boldsymbol{\theta}, \mathbf{x}_{0:t}|\mathbf{y}_{1:t})}{\hat{p}(\mathbf{x}_t|\boldsymbol{\theta}, \mathbf{x}_{t-1}, \mathbf{y}_{1:t}) p(\boldsymbol{\theta}, \mathbf{x}_{0:t-1}|\mathbf{y}_{1:t-1})}.$$

Following the recursive form of $p(\boldsymbol{\theta}, \mathbf{x}_{0:t}|\mathbf{y}_{1:t})$ in (9), we have

$$r_f(\boldsymbol{\theta}, \mathbf{x}_{0:t}) \propto \omega_f(\boldsymbol{\theta}, \mathbf{x}_{t-1:t}) := \frac{f(\mathbf{x}_t|\mathbf{x}_{t-1}, \boldsymbol{\theta}) g(\mathbf{y}_t|\mathbf{x}_t, \boldsymbol{\theta})}{\hat{p}(\mathbf{x}_t|\boldsymbol{\theta}, \mathbf{x}_{t-1}, \mathbf{y}_{1:t})}. \quad (29)$$

Thus, by updating the weights using $W_t^{(i)} = W_{t-1}^{(i)} \omega_f(\widehat{\Theta}^{(i)}, \widehat{\mathbf{X}}_{t-1:t}^{(i)})$ and renormalizing them, i.e., $\{W_t^{(i)}\}_{i=1}^N$, we have the reweighed samples $\{\widehat{\Theta}^{(i)}, \widehat{\mathbf{X}}_{0:t}^{(i)}, W_t^{(i)}\}_{i=1}^N$ that follow the joint posterior density $p(\boldsymbol{\theta}, \mathbf{x}_{0:t} | \mathbf{y}_{1:t})$. Algorithm 3 provides details of the particle filter accompanying the sequential learning procedure in Alg. 2.

Algorithm 3: One iteration of the particle filter accompanying Alg. 2.

- (a) At time $t-1$, suppose we have weighted samples $\{\widehat{\Theta}^{(i)}, \widehat{\mathbf{X}}_{0:t-1}^{(i)}, W_{t-1}^{(i)}\}_{i=1}^N$ following the joint density $p(\boldsymbol{\theta}, \mathbf{x}_{0:t-1} | \mathbf{y}_{1:t-1})$.
- (b) At time t , given the approximate density $\hat{\pi}(\mathbf{x}_t, \boldsymbol{\theta}, \mathbf{x}_{t-1} | \mathbf{y}_{1:t})$ computed in Alg. 2, apply Proposition 2 to integrate $\hat{\pi}$ from the left variable $x_{t,1}$ to the right variable $x_{t,m}$ to define a conditional KR rearrangement $\mathcal{F}_{t,t}^u$ in the form of (26).
- (c) For each of $\{\widehat{\Theta}^{(i)}, \widehat{\mathbf{X}}_{0:t-1}^{(i)}\}_{i=1}^N$, invert $\mathcal{F}_{t,t}^u$ as in (27) to generate a new sample $\widehat{\mathbf{X}}_t^{(i)}$, and then update the weights according to $W_t^{(i)} = W_{t-1}^{(i)} \omega_f(\widehat{\Theta}^{(i)}, \widehat{\mathbf{X}}_{t-1:t}^{(i)})$, where the function $\omega_f(\cdot, \cdot)$ is defined in (29).
- (d) Renormalize the weights $W_t^{(i)} \leftarrow W_t^{(i)} / \sum_{i=1}^N W_t^{(i)}$.

Algorithm 3 can be viewed as an auxiliary particle filter (Pitt and Shephard, 1999) as it uses the next observation to construct the proposal density. Commonly used resampling techniques in sequential Monte Carlo methods can also be used in Alg. 3 as a rejuvenation step to re-balance the weights.

3.4 Path estimation and smoothing

Similar to other particle filter algorithms, weights computed by Alg. 3 may degenerate over time. This has an intuitive explanation in the joint state and parameter estimation context. The locations of the parameter samples are fixed at the initial time, so that the weights (and hence the effective sample size) necessarily degenerate because the parameter posterior may concentrate with more data observed over time. We overcome this issue by drawing random samples from the last approximation $\hat{p}(\mathbf{x}_T, \boldsymbol{\theta}, \mathbf{x}_{T-1} | \mathbf{y}_{1:T})$ —which is conditioned on all available data by construction—and removing the approximation bias by designing a path estimation algorithm accompanying Alg. 2 to replace the particle filtering. The path estimation algorithm also naturally leads to particle smoothing.

Our path estimation algorithm uses the same sequence of non-negative-preserving approximations constructed in Alg. 2. It starts at the final time T and recursively samples backward in time using the lower conditional map $\mathcal{F}_{t,t-1}^l$ defined in (25). At time T , initial samples $\{\widehat{\mathbf{X}}_{T-1}^{(i)}, \widehat{\mathbf{X}}_T^{(i)}, \widehat{\Theta}^{(i)}\}_{i=1}^N$ are generated from $\hat{p}(\mathbf{x}_T, \boldsymbol{\theta}, \mathbf{x}_{T-1} | \mathbf{y}_{1:T})$ using a full KR rearrangement \mathcal{F}_T^l defined in (23). Then, at each of steps $t = T-1, \dots, 1$, for each of $\{\widehat{\Theta}^{(i)}, \widehat{\mathbf{X}}_{t:T}^{(i)}\}_{i=1}^N$, we invert the lower conditional map $\mathcal{F}_{t,t-1}^l$ to obtain

$$\widehat{\mathbf{X}}_{t-1}^{(i)} = (\mathcal{F}_{t,t-1}^l)^{-1}(\Xi_{t-1}^{(i)} | \widehat{\Theta}^{(i)}, \widehat{\mathbf{X}}_t^{(i)}), \quad \Xi_{t-1}^{(i)} \sim \text{uniform}(\boldsymbol{\xi}; [0, 1]^m). \quad (30)$$

Following from Proposition 4, after completing backward recursion, each pair of the parameter sample and state path sample in $\{\hat{\Theta}^{(i)}, \hat{\mathbf{X}}_{0:T}^{(i)}\}_{i=1}^N$ follows the joint density

$$\hat{p}(\boldsymbol{\theta}, \mathbf{x}_{0:T} | \mathbf{y}_{1:T}) = \hat{p}(\mathbf{x}_T, \boldsymbol{\theta}, \mathbf{x}_{T-1} | \mathbf{y}_{1:T}) \prod_{t=1}^{T-1} \hat{p}(\mathbf{x}_{t-1} | \boldsymbol{\theta}, \mathbf{x}_t, \mathbf{y}_{1:t}). \quad (31)$$

Conditioned on $\boldsymbol{\theta}$ and \mathbf{x}_t , the state \mathbf{x}_{t-1} is independent of the data $\mathbf{y}_{t:T}$ observed at future times, and hence we have $p(\mathbf{x}_{t-1} | \boldsymbol{\theta}, \mathbf{x}_t, \mathbf{y}_{1:t}) = p(\mathbf{x}_{t-1} | \boldsymbol{\theta}, \mathbf{x}_t, \mathbf{y}_{1:T})$. Using this identity, the original joint posterior density $p(\boldsymbol{\theta}, \mathbf{x}_{0:T} | \mathbf{y}_{1:T})$ defined in (4) has the same factorized form as the density in (31). Therefore, the above backward sampling procedure can have a reasonable efficiency if the approximations built in Alg. 2 are sufficiently accurate.

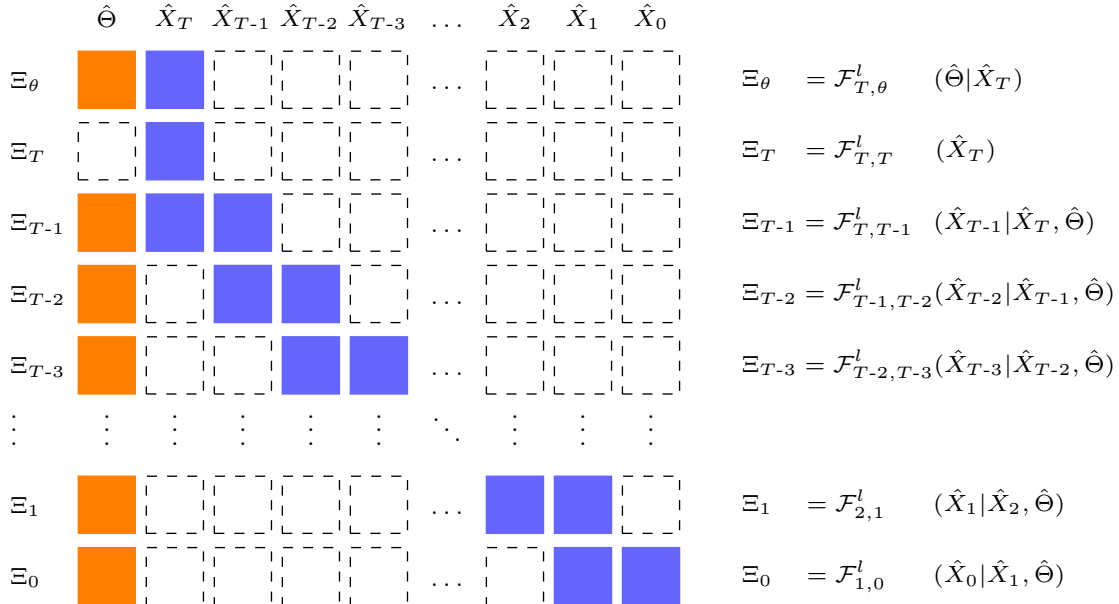


Figure 1: Conditional dependency structures of the joint map \mathcal{F} used in particle smoothing. The blue entries indicate the conditional dependency on the states, the orange entries indicate the conditional dependency on the parameters. The 2×2 sub-matrix in the top left corner represents the structure of the first two blocks of the map \mathcal{F}_T^l .

In fact, the backward recursion can be considered as the inverse of a joint KR rearrangement $\mathcal{F} : \Theta \times \mathcal{X}^{T+1} \rightarrow [0, 1]^{d+(m+1) \times T}$ that transforms approximate posterior random variables $(\hat{\Theta}, \hat{\mathbf{X}}_{0:T} | \mathbf{Y}_{1:T} = \mathbf{y}_{1:T})$ that follow the density (31), to the reference uniform random variables. As illustrated in Figure 1, the joint KR rearrangement \mathcal{F} has a block sparse structure. The non-zero blocks in the first column reflect the conditional dependency of each of the state variables on the parameter, while the non-zero blocks on the first sub-diagonal reflect the Markov dependency of state variables. From this perspective, our TT-based construction of the joint KR rearrangement \mathcal{F} can be viewed as a constructive proof and a numerical implementation of the decomposition theorem (Spantini et al., 2018, Theorem 12) for the joint parameter and state estimation in general state space models. Thus, for

a pair of sample parameter and sample state path ($\widehat{\Theta}^{(i)} = \boldsymbol{\theta}$, $\widehat{\mathbf{X}}_{0:T}^{(i)} = \mathbf{x}_{0:T}$) generated by the backward recursion, it yields a weighted representation of the posterior sample with the importance weight

$$r_b(\boldsymbol{\theta}, \mathbf{x}_{0:T}) = \frac{p(\boldsymbol{\theta}, \mathbf{x}_{0:T} | \mathbf{y}_{1:T})}{\hat{p}(\boldsymbol{\theta}, \mathbf{x}_{0:T} | \mathbf{y}_{1:T})}.$$

Following the recursive form of $p(\boldsymbol{\theta}, \mathbf{x}_{0:t} | \mathbf{y}_{1:t})$, the ratio $r_b(\boldsymbol{\theta}, \mathbf{x}_{0:T})$ has an unnormalized computable form

$$\begin{aligned} r_b(\boldsymbol{\theta}, \mathbf{x}_{0:T}) &\propto \omega_b(\boldsymbol{\theta}, \mathbf{x}_{0:T}) \\ &:= p(\boldsymbol{\theta})p(\mathbf{x}_0 | \boldsymbol{\theta}) \left(\prod_{t=1}^{T-1} \frac{f(\mathbf{x}_t | \mathbf{x}_{t-1}, \boldsymbol{\theta})g(\mathbf{y}_t | \mathbf{x}_t, \boldsymbol{\theta})}{\hat{p}(\mathbf{x}_{t-1} | \boldsymbol{\theta}, \mathbf{x}_t, \mathbf{y}_{1:t})} \right) \frac{f(\mathbf{x}_T | \mathbf{x}_{T-1}, \boldsymbol{\theta})g(\mathbf{y}_T | \mathbf{x}_T, \boldsymbol{\theta})}{\hat{p}(\mathbf{x}_T, \boldsymbol{\theta}, \mathbf{x}_{T-1} | \mathbf{y}_{1:T})}. \end{aligned} \quad (32)$$

We summarize the particle smoothing procedure in Alg. 4. The set of weighted samples $\{\widehat{\Theta}^{(i)}, \widehat{\mathbf{X}}_{0:T}^{(i)}, W^{(i)}\}_{i=1}^N$ is an unbiased representation of the joint posterior random variables $(\boldsymbol{\Theta}, \mathbf{X}_{0:T} | \mathbf{y}_{1:T})$. It mitigates the particle degeneracy because the samples are drawn conditioned all observed data $\mathbf{y}_{1:T}$.

Algorithm 4: Path estimation algorithm accompanying Alg. 2.

- Generate samples $\{\widehat{\mathbf{X}}_T^{(i)}, \widehat{\Theta}^{(i)}, \widehat{\mathbf{X}}_{T-1}^{(i)}\}_{i=1}^N$ from $\hat{p}(\mathbf{x}_T, \boldsymbol{\theta}, \mathbf{x}_{T-1} | \mathbf{y}_{1:T})$ using \mathcal{F}_T^l .
- For $t = T-1, \dots, 1$, do the following
 - For each of $\{\widehat{\Theta}^{(i)}, \widehat{\mathbf{X}}_{t:T}^{(i)}\}_{i=1}^N$, invert the lower conditional map $\mathcal{F}_{t,t-1}^l$ as in (30) to generate a new sample $\widehat{\mathbf{X}}_{t-1}^{(i)}$.
- For each of $\{\widehat{\Theta}^{(i)}, \widehat{\mathbf{X}}_{0:T}^{(i)}\}_{i=1}^N$, compute the weight $W^{(i)}$ using (32).
- Normalize the weights as $W^{(i)} \leftarrow W^{(i)} / \sum_{i=1}^N W^{(i)}$.

In our setting, applying one step of particle filtering and one step of particle smoothing have the same computational complexity. For particle filtering, integrations used for constructing the upper conditional map $\mathcal{F}_{t,t}^u$ in (26) takes the opposite direction to the integrations used for building $\hat{\pi}(\mathbf{x}_t, \boldsymbol{\theta} | \mathbf{y}_{1:t})$ in Alg. 2. This incurs an additional $\mathcal{O}(mlr^3)$ floating point operations. In comparison, constructing the lower conditional map $\mathcal{F}_{t,t-1}^l$ in (25) for particle smoothing share the same integrations as in Alg. 2, and thus does not incur additional computational cost.

Marginalizing the square TT approximation (22) from either end has an $\mathcal{O}(\ell r^3)$ computational complexity per coordinate. This is much lower than marginalizing variables in the middle, which has an $\mathcal{O}(\ell r^6)$ computational complexity per coordinate. Thus, the variable ordering $(\mathbf{x}_t, \boldsymbol{\theta}, \mathbf{x}_{t-1})$ is computationally advantageous for both smoothing and filtering. One can also consider the variable ordering $(\boldsymbol{\theta}, \mathbf{x}_t, \mathbf{x}_{t-1})$ if only the smoothing algorithm is used for debiasing, as Alg. 2 and the lower conditional map in Alg. 4 only need to integrate the state \mathbf{x}_{t-1} .

4 Error analysis

The central element of Alg. 1 and 2 is the recursive approximation of the unnormalized joint densities of the posterior random variables $(\mathbf{X}_t, \boldsymbol{\Theta}, \mathbf{X}_{t-1} | \mathbf{Y}_{1:t} = \mathbf{y}_{1:t})$ using TT decompositions. Here we analyze the accumulation of approximation errors in TT-based algorithms. Since Alg. 1 and 2 share a similar recursive structure, we first outline the notation, assumptions and key steps of our analysis, and then discuss the details.

4.1 Error decomposition

Starting with the initial unnormalized joint posterior density

$$\pi(\mathbf{x}_1, \boldsymbol{\theta}, \mathbf{x}_0 | \mathbf{y}_1) = p(\boldsymbol{\theta}) p(\mathbf{x}_0 | \boldsymbol{\theta}) f(\mathbf{x}_1 | \mathbf{x}_0, \boldsymbol{\theta}) g(\mathbf{y}_1 | \mathbf{x}_1, \boldsymbol{\theta}),$$

we define the unnormalized joint posterior density recursively as

$$\begin{aligned} \pi(\mathbf{x}_t, \boldsymbol{\theta}, \mathbf{x}_{t-1} | \mathbf{y}_{1:t}) &= \int \pi(\mathbf{x}_{t-1}, \boldsymbol{\theta}, \mathbf{x}_{t-2} | \mathbf{y}_{1:t-1}) d\mathbf{x}_{t-2} f(\mathbf{x}_t | \mathbf{x}_{t-1}, \boldsymbol{\theta}) g(\mathbf{y}_t | \mathbf{x}_t, \boldsymbol{\theta}) \\ &= \pi(\mathbf{x}_{t-1}, \boldsymbol{\theta} | \mathbf{y}_{1:t-1}) f(\mathbf{x}_t | \mathbf{x}_{t-1}, \boldsymbol{\theta}) g(\mathbf{y}_t | \mathbf{x}_t, \boldsymbol{\theta}), \end{aligned}$$

which follows from a similar derivation to that of (10). We use shorthands $p_t(\mathbf{x}_t, \boldsymbol{\theta}, \mathbf{x}_{t-1}) := p(\mathbf{x}_t, \boldsymbol{\theta}, \mathbf{x}_{t-1} | \mathbf{y}_{1:t})$ and $\hat{p}_t(\mathbf{x}_t, \boldsymbol{\theta}, \mathbf{x}_{t-1}) := \hat{p}(\mathbf{x}_t, \boldsymbol{\theta}, \mathbf{x}_{t-1} | \mathbf{y}_{1:t})$ to respectively denote the joint posterior density at time t and its TT-based approximation. Similar notation is adopted for representing their unnormalized counterparts. We omit the input variables when no confusion arises. The density π_t has the normalizing constant $z_t := \int \pi(\mathbf{x}_t, \boldsymbol{\theta}, \mathbf{x}_{t-1} | \mathbf{y}_{1:t}) d\mathbf{x}_t d\boldsymbol{\theta} d\mathbf{x}_{t-1} =: p(\mathbf{y}_{1:t})$, where $p(\mathbf{y}_{1:t})$ is defined in (9).

Recall that in each iteration of Alg. 1 and 2, the unnormalized joint posterior density π_t can not be directly evaluated since it is the density of marginal random variables. Instead, we introduce the non-separable, unnormalized approximation q_t in step (a) of both algorithms, and then approximate q_t using a TT-based approximation $\hat{\pi}_t$ in step (b). As shown in (14) and (20), the function q_t takes the form

$$q_t(\mathbf{x}_t, \boldsymbol{\theta}, \mathbf{x}_{t-1}) = \hat{\pi}(\mathbf{x}_{t-1}, \boldsymbol{\theta} | \mathbf{y}_{1:t-1}) f(\mathbf{x}_t | \mathbf{x}_{t-1}, \boldsymbol{\theta}) g(\mathbf{y}_t | \mathbf{x}_t, \boldsymbol{\theta}),$$

where $\hat{\pi}(\mathbf{x}_{t-1}, \boldsymbol{\theta} | \mathbf{y}_{1:t-1})$ is the marginalization of the previous TT-based approximation. The construction of the function q_t enables pointwise function evaluations that are necessary for building the new TT decomposition used by $\hat{\pi}_t$.

This reveals that each iteration of Alg. 1 and 2 can be considered as a two-step approximation procedure: The unnormalized joint density π_t is approximated by the function q_t , from which we construct the TT-based approximation $\hat{\pi}_t$. Considering some distance metric $D(\cdot, \cdot)$, the error $D(\hat{\pi}_t, \pi_t)$ has the decomposition

$$D(\hat{\pi}_t, \pi_t) \leq D(\hat{\pi}_t, q_t) + D(q_t, \pi_t) \tag{33}$$

using the triangle inequality, where $D(\hat{\pi}_t, q_t)$ is the *approximation error* in the current iteration and $D(q_t, \pi_t)$ is the *propagation error* from the previous iteration. We aim to understand how the approximation errors accumulate over time in the recursive algorithms. We adopt the following assumptions to analyze the propagation error.

Assumption 1 For the state transition and observation processes, we assume either of the following bounds holds

$$C_t^{(g)} = \sup_{\mathbf{x}_t \in \mathcal{X}, \boldsymbol{\theta} \in \Theta} g(\mathbf{y}_t | \mathbf{x}_t, \boldsymbol{\theta}) < \infty, \quad (34)$$

$$C_t^{(f)} = \sup_{\mathbf{x}_{t-1} \in \mathcal{X}, \boldsymbol{\theta} \in \Theta} \int f(\mathbf{x}_t | \mathbf{x}_{t-1}, \boldsymbol{\theta}) g(\mathbf{y}_t | \mathbf{x}_t, \boldsymbol{\theta}) d\mathbf{x}_t < \infty. \quad (35)$$

Generally speaking, any Lipschitz continuous f and g satisfy the above assumptions, which are usually the case in many applications. For example, an observation model with the commonly used Gaussian noise has a bounded $C_t^{(g)}$ for all t .

4.2 Error analysis for Alg. 1

Algorithm 1 direct builds the approximation $\hat{\pi}_t$ using a TT decomposition. The approximation does not preserve non-negativity, and hence common statistical divergences cannot be used to bound the error. In this case, we use the L^1 norm as the distance metric, which is analogous to the total variation distance of probability measures. In the following, we show in Proposition 5 that the approximation error $\|\hat{\pi}_t - q_t\|_{L^1}$ can be bounded based on certain Sobolev-type smoothness assumptions. Then, we bound the propagation error $\|q_t - \pi_t\|_{L^1}$ and the total error $\|\hat{\pi}_t - \pi_t\|_{L^1}$ in Proposition 7 and Theorem 8, respectively.

Proposition 5 For any time $t > 0$, we express the product of the state transition density and the likelihood function as

$$h_t(\mathbf{x}_t, \boldsymbol{\theta}, \mathbf{x}_{t-1}) = f(\mathbf{x}_t | \mathbf{x}_{t-1}, \boldsymbol{\theta}) g(\mathbf{y}_t | \mathbf{x}_t, \boldsymbol{\theta}).$$

We assume that state space \mathcal{X} and the parameter space Θ are compact in the sense that they admit finite Lebesgue measures and there exist some $K \in \mathbb{N}$ and $s \geq 1$ such that $h_t \in W^{K+1,2s}(\mathcal{X} \times \Theta \times \mathcal{X})$. At time $t = 1$, we further assume that the (unnormalized) prior density $\pi(\mathbf{x}_0, \boldsymbol{\theta}) := \pi(\mathbf{x}_0 | \boldsymbol{\theta}) \pi(\boldsymbol{\theta})$ belongs to $W^{K+1,2r}(\mathcal{X} \times \Theta)$ for some $r \geq 1$ such that $\frac{1}{r} + \frac{1}{s} = 1$. Then, for some target error threshold $\varepsilon_t \in (0, 1)$ at time $t > 0$, there exists a TT decomposition $\hat{\pi}_t(\mathbf{x}_t, \boldsymbol{\theta}, \mathbf{x}_{t-1})$ with ranks

$$r_1 = \lceil \varepsilon_t^{-1/K} \rceil \quad \text{and} \quad r_k = \lceil \varepsilon_t^{-k/K} \rceil \quad \text{for } k = 2, 3, \dots, 2m + d - 1, \quad (36)$$

such that the approximation error in step (b) of Alg. 1 is bounded by

$$\|\hat{\pi}_t - q_t\|_{L^1} \lesssim \sqrt{\Omega(\mathcal{X} \times \Theta \times \mathcal{X})(2m + d - 1)} \varepsilon_t,$$

where $\Omega(\cdot)$ denotes the volume of space and $C \lesssim D$ denotes that C is bounded by a multiple of D independently of parameters which C and D may depend on.

Proof Our goal is to establish the Sobolev-type smoothness of the function q_t , so that results of Griebel and Harbrecht (2023) can be used to derive the TT ranks for some target error measured in the L^2 norm. The bound on the L^1 norm follows from that on the L^2 norm using the Cauchy–Schwartz inequality.

For brevity, we define the previous marginal density $\hat{\pi}(\mathbf{x}_{t-1}, \boldsymbol{\theta} | \mathbf{y}_{1:t-1})$ as

$$\hat{\varphi}_t(\mathbf{x}_t, \boldsymbol{\theta}, \mathbf{x}_{t-1}) = \begin{cases} \hat{\pi}(\mathbf{x}_{t-1}, \boldsymbol{\theta} | \mathbf{y}_{1:t-1}), & t > 1 \\ \pi(\mathbf{x}_0, \boldsymbol{\theta}), & t = 1 \end{cases},$$

which takes a constant value over \mathbf{x}_t . For $t > 1$, since the marginal TT approximation $\hat{\pi}(\mathbf{x}_{t-1}, \boldsymbol{\theta} | \mathbf{y}_{1:t-1})$ is a linear combination of multivariate polynomial basis functions, the function $\hat{\varphi}_t$ is an analytical function. Thus, we have $\hat{\varphi}_t \in W^{K+1,2r}(\mathcal{X} \times \Theta \times \mathcal{X})$ for any $K \in \mathbb{N}$, $r \geq 1/2$, and $t > 1$.

For $t > 0$, the L^2 norm of q_t can be expressed as $\|q_t\|_{L^2}^2 = \|\hat{\varphi}_t^2 h_t^2\|_{L^1}$. Applying the Hölder inequality, we have

$$\|q_t\|_{L^2} \leq \|\hat{\varphi}_t^2\|_{L^r}^{1/2} \|h_t^2\|_{L^s}^{1/2} = \|\hat{\varphi}_t\|_{L^{2r}} \|h_t\|_{L^{2s}}$$

for $r, s \in [0, \infty]$ with $\frac{1}{r} + \frac{1}{s} = 1$. This way, we have $\|q_t\|_{L^2} < \infty$ for all $t > 0$ by our assumptions and the analyticity of $\hat{\varphi}_t$ for $t > 1$. For derivatives of q_t , with the multi-index notation and the general Leibniz rule (see Constantine and Savits (1996)), we have

$$\partial^{\boldsymbol{\alpha}} q_t = \sum_{\boldsymbol{\beta} \leq \boldsymbol{\alpha}} \binom{\boldsymbol{\alpha}}{\boldsymbol{\beta}} (\partial^{\boldsymbol{\alpha}-\boldsymbol{\beta}} \hat{\varphi}_t) (\partial^{\boldsymbol{\beta}} h_t),$$

where $\boldsymbol{\alpha}, \boldsymbol{\beta}$ are multi-indices. Following a similar derivation as in the L_2 norm case, we can show that $\|\partial^{\boldsymbol{\alpha}} q_t\|_{L^2} < \infty$ for all $|\boldsymbol{\alpha}| \leq K + 1$, where $|\boldsymbol{\alpha}| = \sum \alpha_i$. Therefore, we have $q_t \in W^{K+1,2}(\mathcal{X} \times \Theta \times \mathcal{X})$ for all $t > 0$.

Given a target error threshold $\varepsilon_t \in (0, 1)$, Theorem 4 of Griebel and Harbrecht (2023) states that there exists a TT decomposition $\hat{\pi}_t$ with ranks $r_1 = \lceil \varepsilon_t^{-1/K} \rceil$ and $r_k = \lceil \varepsilon_t^{-2k/K} \rceil$ for $k = 2, 3, \dots, 2m+d-1$ such that $\|\hat{\pi}_t - q_t\|_{L^2} \lesssim \sqrt{2m+d-1} \varepsilon_t$. Then, by the Cauchy–Schwartz inequality, we have

$$\|\hat{\pi}_t - q_t\|_{L^1} \leq \sqrt{\Omega(\mathcal{X} \times \Theta \times \mathcal{X})} \|\hat{\pi}_t - q_t\|_{L^2},$$

and thus the result follows. ■

Remark 6 Proposition 5 only considers bounded spaces. This can be easily extended to unbounded spaces by considering a weight measure and a slightly modified approximation scheme. See Cui and Dolgov (2022); Cui et al. (2023) and references therein for details. The result of Griebel and Harbrecht (2023) establishes sufficient conditions of the a priori error bound of TT decompositions using smoothness. In practice, there are many examples of low-rank functions that do not satisfy the smoothness assumption, e.g., products of discontinuous univariate functions. To the authors' knowledge, the analysis of TT ranks for general functions is still an active research area and the results of Griebel and Harbrecht (2023) may not provide a precise practical guideline for building TT decompositions. Nonetheless, Proposition 5 provides some confidence in applying TT decompositions in the sequential state and parameter learning problems.

Proposition 7 Suppose either bound of Assumption 1 holds. The propagation error $\|q_t - \pi_t\|_{L^1}$ in time t is bounded by the previous total error

$$\|q_t - \pi_t\|_{L^1} \leq C_t^{(h)} \|\hat{\pi}_{t-1} - \pi_{t-1}\|_{L^1}, \quad h \in \{f, g\}. \quad (37)$$

Proof By the construction of q_t , we express the propagation error as

$$\|q_t - \pi_t\|_{L^1} = \int \left| \hat{\pi}(\mathbf{x}_{t-1}, \boldsymbol{\theta} | \mathbf{y}_{1:t-1}) - \pi(\mathbf{x}_{t-1}, \boldsymbol{\theta} | \mathbf{y}_{1:t-1}) \right| r(\mathbf{x}_{t-1}, \boldsymbol{\theta}) d\mathbf{x}_{t-1} d\boldsymbol{\theta}, \quad (38)$$

where $r(\mathbf{x}_{t-1}, \boldsymbol{\theta}) = \int f(\mathbf{x}_t | \mathbf{x}_{t-1}, \boldsymbol{\theta}) g(\mathbf{y}_t | \mathbf{x}_t, \boldsymbol{\theta}) d\mathbf{x}_t$. Either assumption (34) or (35) leads to $\sup_{\mathbf{x}_{t-1} \in \mathcal{X}, \boldsymbol{\theta} \in \Theta} r(\mathbf{x}_{t-1}, \boldsymbol{\theta}) \leq C_t^{(h)}$ for $h \in \{f, g\}$, and thus we have

$$\|q_t - \pi_t\|_{L^1} \leq C_t^{(h)} \|\hat{\pi}(\mathbf{x}_{t-1}, \boldsymbol{\theta} | \mathbf{y}_{1:t-1}) - \pi(\mathbf{x}_{t-1}, \boldsymbol{\theta} | \mathbf{y}_{1:t-1})\|_{L^1}.$$

Applying Lemma 16, the L^1 distance of the marginal densities is bounded by that of the joint densities as

$$\|\hat{\pi}(\mathbf{x}_{t-1}, \boldsymbol{\theta} | \mathbf{y}_{1:t-1}) - \pi(\mathbf{x}_{t-1}, \boldsymbol{\theta} | \mathbf{y}_{1:t-1})\|_{L^1} \leq \|\hat{\pi}_{t-1} - \pi_{t-1}\|_{L^1},$$

which leads to the result. \blacksquare

Theorem 8 Suppose either bound of Assumption 1 holds and the TT decomposition in step (b) of Alg. 1 satisfies $\|\hat{\pi}_t - q_t\|_{L^1} \leq \epsilon_t$. For $t > 0$, the total error satisfies

$$\|\hat{\pi}_t - \pi_t\|_{L^1} \leq C_t^{(h)} \|\pi_{t-1} - \hat{\pi}_{t-1}\|_{L^1} + \epsilon_t \leq \sum_{k=1}^t C^{t-k} \epsilon_k,$$

for $h \in \{f, g\}$, where $C = \sup_t C_t^{(h)}$.

Proof The result follows from the triangle inequality (33) and induction. \blacksquare

4.3 Stability of Alg. 2

Since the TT-based approximation used in Alg. 2 preserves non-negativity of density functions by factorizing the square root of the function q_t , here we focus on deriving bounds on the Hellinger divergence of the resulting approximations. Applying Lemma 1, in each iteration of Alg. 2, the Hellinger distance between \hat{p}_t and p_t is bounded by the L^2 distance between $\sqrt{\hat{\pi}_t}$ and $\sqrt{\pi_t}$, i.e.,

$$D_H(\hat{p}_t, p_t) \leq \frac{\sqrt{2}}{\sqrt{z_t}} \|\sqrt{\hat{\pi}_t} - \sqrt{\pi_t}\|_{L^2}. \quad (39)$$

Thus, it is sufficient for us to consider the accumulation of $\|\sqrt{\hat{\pi}_t} - \sqrt{\pi_t}\|_{L^2}$, which also follows the decomposition shown in (33). In the following, we bound the approximation error $\|\sqrt{\hat{\pi}_t} - \sqrt{q_t}\|_{L^2}$ in Proposition 9—we omit the proof as it is a direct consequence of Lemma 1. Then, we bound the propagation error $\|\sqrt{q_t} - \sqrt{\pi_t}\|_{L^2}$ and the total error $\|\sqrt{\hat{\pi}_t} - \sqrt{\pi_t}\|_{L^2}$ in Proposition 11 and Theorem 12, respectively.

Proposition 9 *In each iteration of Alg. 2, suppose the TT decomposition ϕ_t has an L^2 error that satisfies $\|\phi_t - \sqrt{q_t}\|_{L^2} < \epsilon_t$ and the constant τ_t satisfies $\tau_t \leq \|\phi_t - \sqrt{q_t}\|_{L^2}^2$. Then, the approximation error satisfies $\|\sqrt{\hat{\pi}_t} - \sqrt{q_t}\|_{L^2} \leq \sqrt{2}\epsilon_t$.*

Remark 10 *In Alg. 2, the previous marginal density, $\hat{\pi}(\mathbf{x}_{t-1}, \boldsymbol{\theta} | \mathbf{y}_{1:t-1})$, can be expressed as a sum of squares of multivariate polynomial functions (each in the TT form) together with a defensive term to ensure the non-negativity (cf. Proposition 2). Applying the multivariate Faa di Bruno formula (Constantine and Savits, 1996), one can show that the square root of the previous marginal density, $\sqrt{\hat{\pi}(\mathbf{x}_{t-1}, \boldsymbol{\theta} | \mathbf{y}_{1:t-1})}$, yields a bounded Sobolev norm for a finite order of differentiability K . But the bound on the Sobolev norm may increase with K . Although Theorem 4 of Griebel and Harbrecht (2023) may still apply in this case for a finite K , it requires further analysis to understand the impact of increasing Sobolev norm on the a priori error analysis of the TT decomposition. In our numerical examples (cf. Section 6.1), we demonstrate that Alg. 1 and 2 achieve comparable approximation accuracy.*

Proposition 11 *Suppose either bound of Assumption 1 holds. The propagation error $\|\sqrt{q_t} - \sqrt{\pi_t}\|_{L^2}$ at time t is bounded by the previous total error*

$$\|\sqrt{q_t} - \sqrt{\pi_t}\|_{L^2} \leq \sqrt{C_t^{(h)}} \|\sqrt{\hat{\pi}_{t-1}} - \sqrt{\pi_{t-1}}\|_{L^2}, \quad h \in \{f, g\}. \quad (40)$$

Proof By the construction of q_t , we express the squared propagation error as

$$\|\sqrt{q_t} - \sqrt{\pi_t}\|_{L^2}^2 = \int \left(\sqrt{\hat{\pi}(\mathbf{x}_{t-1}, \boldsymbol{\theta} | \mathbf{y}_{1:t-1})} - \sqrt{\pi(\mathbf{x}_{t-1}, \boldsymbol{\theta} | \mathbf{y}_{1:t-1})} \right)^2 r(\mathbf{x}_{t-1}, \boldsymbol{\theta}) d\mathbf{x}_{t-1} d\boldsymbol{\theta}, \quad (41)$$

where $r(\mathbf{x}_{t-1}, \boldsymbol{\theta}) = \int f(\mathbf{x}_t | \mathbf{x}_{t-1}, \boldsymbol{\theta}) g(\mathbf{y}_t | \mathbf{x}_t, \boldsymbol{\theta}) d\mathbf{x}_t$. Either assumption (34) or (35) leads to $\sup_{\mathbf{x}_{t-1} \in \mathcal{X}, \boldsymbol{\theta} \in \Theta} r(\mathbf{x}_{t-1}, \boldsymbol{\theta}) \leq C_t^{(h)}$ for $h \in \{f, g\}$, and thus we have

$$\begin{aligned} \|\sqrt{q_t} - \sqrt{\pi_t}\|_{L^2}^2 &\leq C_t^{(h)} \int \left(\sqrt{\hat{\pi}(\mathbf{x}_{t-1}, \boldsymbol{\theta} | \mathbf{y}_{1:t-1})} - \sqrt{\pi(\mathbf{x}_{t-1}, \boldsymbol{\theta} | \mathbf{y}_{1:t-1})} \right)^2 d\mathbf{x}_{t-1} d\boldsymbol{\theta} \\ &= C_t^{(h)} \left\| \sqrt{\hat{\pi}(\mathbf{x}_{t-1}, \boldsymbol{\theta} | \mathbf{y}_{1:t-1})} - \sqrt{\pi(\mathbf{x}_{t-1}, \boldsymbol{\theta} | \mathbf{y}_{1:t-1})} \right\|_{L^2}^2. \end{aligned}$$

Applying Lemma 15, the L^2 distance for the marginal densities is bounded by that for the joint densities as

$$\left\| \sqrt{\hat{\pi}(\mathbf{x}_{t-1}, \boldsymbol{\theta} | \mathbf{y}_{1:t-1})} - \sqrt{\pi(\mathbf{x}_{t-1}, \boldsymbol{\theta} | \mathbf{y}_{1:t-1})} \right\|_{L^2} \leq \|\sqrt{\hat{\pi}_{t-1}} - \sqrt{\pi_{t-1}}\|_{L^2}$$

Taking square root of both sides of the above equation gives the result. ■

Theorem 12 *Suppose the assumptions of Proposition 9 and either bound of Assumption 1 hold. For $t > 0$, the total error of Alg. 2 satisfies*

$$\|\sqrt{\hat{\pi}_t} - \sqrt{\pi_t}\|_{L^2} \leq \sqrt{C_t^{(h)}} \|\sqrt{\pi_{t-1}} - \sqrt{\hat{\pi}_{t-1}}\|_{L^2} + \sqrt{2}\epsilon_t, \quad h \in \{f, g\},$$

and the Hellinger distance between p_t and its approximation \hat{p}_t is bounded by

$$D_H(\hat{p}_t, p_t) \leq \frac{2}{\sqrt{p(\mathbf{y}_{1:t})}} \sum_{k=1}^t C^{(t-k)/2} \epsilon_k, \quad C = \sup_t C_t^{(h)}.$$

Proof The first result directly follows from the triangle inequality (33). For the second result, we recall that there is no approximation used in Alg. 2 at t_0 , i.e., $\epsilon_0 = 0$, as we only have the prior for \mathbf{X}_0 and Θ . Applying the first result and induction, we have $\|\sqrt{\hat{\pi}_t} - \sqrt{\pi_t}\|_{L^2} \leq \sqrt{2 \sum_{k=1}^t C^{(t-k)/2} \epsilon_k}$. Since $z_t = p(\mathbf{y}_{1:t})$ by definition, the second result follows from the identity in (39). \blacksquare

Remark 13 We need to marginalize the approximation $\hat{p}(\mathbf{x}_t, \boldsymbol{\theta}, \mathbf{x}_{t-1} | \mathbf{y}_{1:t})$ to obtain approximations of the filtering density $p(\mathbf{x}_t | \mathbf{y}_{1:t})$ and the parameter posterior density $p(\boldsymbol{\theta} | \mathbf{y}_{1:t})$. By Lemma 14, the Hellinger distances between marginals and their corresponding approximations can not exceed the Hellinger error of joint densities presented in Theorem 12.

5 Preconditioning methods

The key step of Alg. 2 is to approximate the square root of the non-separable, unnormalized density q_t by a TT decomposition $\phi_{q,t}$. In many applications, the temporally increasing data size and complex nonlinear interactions among parameters and states may concentrate posterior densities to some submanifold, and hence result in potentially high ranks in $\phi_{q,t}$. This can make the TT-based algorithms computationally demanding. Rather than directly approximating q_t , here we present a preconditioning framework to improve TT's approximation efficiency and discuss how to apply the resulting preconditioned approximations in our sequential estimation algorithms (cf. Alg. 2–4).

5.1 General framework

Our preconditioning procedure is guided by a (possibly unnormalized) bridging density $\rho_t(\mathbf{x}_t, \boldsymbol{\theta}, \mathbf{x}_{t-1})$ that is easier to approximate than $q_t(\mathbf{x}_t, \boldsymbol{\theta}, \mathbf{x}_{t-1})$. We introduce general reference random variables $(\mathbf{U}_t, \mathbf{U}_\theta, \mathbf{U}_{t-1})$ with tensor-product normalized density $\eta(\mathbf{u}_t, \mathbf{u}_\theta, \mathbf{u}_{t-1}) = \eta(\mathbf{u}_t)\eta(\mathbf{u}_\theta)\eta(\mathbf{u}_{t-1})$, where $(\mathbf{U}_t, \mathbf{U}_{t-1})$ take values in \mathbb{R}^m and \mathbf{U}_θ takes values \mathbb{R}^d . The preconditioning has the following conceptual steps.

1. **Change of coordinates.** We first construct a *preconditioning KR rearrangement* \mathcal{T}_t such that

$$(\mathcal{T}_t)_\sharp \rho_t(\mathbf{u}_t, \mathbf{u}_\theta, \mathbf{u}_{t-1}) = \rho_t(\mathcal{T}_t^{-1}(\mathbf{u}_t, \mathbf{u}_\theta, \mathbf{u}_{t-1})) |\nabla \mathcal{T}_t^{-1}(\mathbf{u}_t, \mathbf{u}_\theta, \mathbf{u}_{t-1})| \propto \eta(\mathbf{u}_t, \mathbf{u}_\theta, \mathbf{u}_{t-1}). \quad (42)$$

The map \mathcal{T}_t defines a change of coordinates from $(\mathbf{x}_t, \boldsymbol{\theta}, \mathbf{x}_{t-1})$ to $(\mathbf{u}_t, \mathbf{u}_\theta, \mathbf{u}_{t-1})$.

2. **Preconditioning.** Applying the identity in (42), the pushforward of q_t under \mathcal{T}_t takes form

$$(\mathcal{T}_t)_\sharp q_t(\mathbf{u}_t, \mathbf{u}_\theta, \mathbf{u}_{t-1}) = q_t(\mathcal{T}_t^{-1}(\mathbf{u}_t, \mathbf{u}_\theta, \mathbf{u}_{t-1})) |\nabla \mathcal{T}_t^{-1}(\mathbf{u}_t, \mathbf{u}_\theta, \mathbf{u}_{t-1})| \propto q_{\sharp,t}(\mathbf{u}_t, \mathbf{u}_\theta, \mathbf{u}_{t-1}), \quad (43)$$

where

$$q_{\sharp,t}(\mathbf{u}_t, \mathbf{u}_\theta, \mathbf{u}_{t-1}) := \frac{q_t(\mathcal{T}_t^{-1}(\mathbf{u}_t, \mathbf{u}_\theta, \mathbf{u}_{t-1}))}{\rho_t(\mathcal{T}_t^{-1}(\mathbf{u}_t, \mathbf{u}_\theta, \mathbf{u}_{t-1}))} \eta(\mathbf{u}_t, \mathbf{u}_\theta, \mathbf{u}_{t-1}) \quad (44)$$

is a non-negative function that can be evaluated pointwise. The pushforward density $q_{\sharp,t}$ can be viewed as the reference density η perturbed by the ratio q_t/ρ_t in the transformed coordinates $(\mathbf{u}_t, \mathbf{u}_\theta, \mathbf{u}_{t-1})$. With a suitable bridging density, the ratio q_t/ρ_t is significantly less concentrated, and hence may be easier to approximate. See Fig. 2 for an illustration.

3. TT-approximation. By approximating $\sqrt{q_{\sharp,t}}$ using a TT $\phi_{\sharp,t}$, i.e.,

$$\sqrt{q_{\sharp,t}(\mathbf{u}_t, \mathbf{u}_\theta, \mathbf{u}_{t-1})} \approx \phi_{\sharp,t}(\mathbf{u}_t, \mathbf{u}_\theta, \mathbf{u}_{t-1}), \quad (45)$$

we can follow the squared-TT approximation outlined in Section 3.1 to define an unnormalized approximate density

$$\hat{\nu}_{\sharp,t}(\mathbf{u}_t, \mathbf{u}_\theta, \mathbf{u}_{t-1}) := \phi_{\sharp,t}(\mathbf{u}_t, \mathbf{u}_\theta, \mathbf{u}_{t-1})^2 + \tau_{\sharp,t}\eta(\mathbf{u}_t, \mathbf{u}_\theta, \mathbf{u}_{t-1}) \quad (46)$$

where $\tau_{\sharp,t} \leq \|\phi_{\sharp,t} - \sqrt{q_{\sharp,t}}\|_{L^2}^2$. Applying Proposition 2 and denoting the normalized density by $\hat{\mu}_{\sharp,t} \propto \hat{\nu}_{\sharp,t}$, we obtain a KR rearrangement \mathcal{S}_t such that

$$(\mathcal{S}_t)_{\sharp} \hat{\mu}_{\sharp,t}(\boldsymbol{\xi}_t, \boldsymbol{\xi}_\theta, \boldsymbol{\xi}_{t-1}) = \text{uniform}(\boldsymbol{\xi}_t, \boldsymbol{\xi}_\theta, \boldsymbol{\xi}_{t-1}).$$

4. Composition. The above steps define a composite transformation $\mathcal{S}_t \circ \mathcal{T}_t$ that approximately pushes forward the normalized version of the density $q_t(\mathbf{x}_t, \boldsymbol{\theta}, \mathbf{x}_{t-1})$ to a uniform density. Equivalently, we have

$$q_t(\mathbf{x}_t, \boldsymbol{\theta}, \mathbf{x}_{t-1}) \propto (\mathcal{S}_t \circ \mathcal{T}_t)^{\sharp} \text{uniform}(\mathbf{x}_t, \boldsymbol{\theta}, \mathbf{x}_{t-1}). \quad (47)$$

Thus, the pullback of the uniform density under $\mathcal{S}_t \circ \mathcal{T}_t$ defines a normalized approximate posterior density, which takes the form

$$\begin{aligned} \hat{p}(\mathbf{x}_t, \boldsymbol{\theta}, \mathbf{x}_{t-1} | \mathbf{y}_{1:t}) &= (\mathcal{S}_t \circ \mathcal{T}_t)^{\sharp} \text{uniform}(\mathbf{x}_t, \boldsymbol{\theta}, \mathbf{x}_{t-1}) \\ &= |\nabla(\mathcal{S}_t \circ \mathcal{T}_t)(\mathbf{x}_t, \boldsymbol{\theta}, \mathbf{x}_{t-1})| \\ &\stackrel{(42)}{=} \frac{\hat{\mu}_{\sharp,t}(\mathcal{T}_t(\mathbf{x}_t, \boldsymbol{\theta}, \mathbf{x}_{t-1}))}{\eta(\mathcal{T}_t(\mathbf{x}_t, \boldsymbol{\theta}, \mathbf{x}_{t-1}))} \rho_t(\mathbf{x}_t, \boldsymbol{\theta}, \mathbf{x}_{t-1}) \\ &= \frac{1}{\hat{z}_t} \hat{\pi}(\mathbf{x}_t, \boldsymbol{\theta}, \mathbf{x}_{t-1} | \mathbf{y}_{1:t}), \end{aligned} \quad (48)$$

where

$$\hat{\pi}(\mathbf{x}_t, \boldsymbol{\theta}, \mathbf{x}_{t-1} | \mathbf{y}_{1:t}) = \frac{\hat{\nu}_{\sharp,t}(\mathcal{T}_t(\mathbf{x}_t, \boldsymbol{\theta}, \mathbf{x}_{t-1}))}{\eta(\mathcal{T}_t(\mathbf{x}_t, \boldsymbol{\theta}, \mathbf{x}_{t-1}))} \rho_t(\mathbf{x}_t, \boldsymbol{\theta}, \mathbf{x}_{t-1}) \quad (49)$$

is the unnormalized approximate posterior density and

$$\hat{z}_t = \int \hat{\pi}(\mathbf{x}_t, \boldsymbol{\theta}, \mathbf{x}_{t-1} | \mathbf{y}_{1:t}) d\mathbf{x}_t d\boldsymbol{\theta} d\mathbf{x}_{t-1} = \int \hat{\nu}_{\sharp,t}(\mathbf{u}_t, \mathbf{u}_\theta, \mathbf{u}_{t-1}) d\mathbf{u}_t d\mathbf{u}_\theta d\mathbf{u}_{t-1},$$

is the normalizing constant. The last equality follows from the change of coordinates defined by \mathcal{T}_t .

There are many ways to defining the bridging density ρ_t and building the preconditioning map \mathcal{T}_t . In the following, we provide some examples of bridging densities relying on the particular structure of q_t , which is defined in (20).

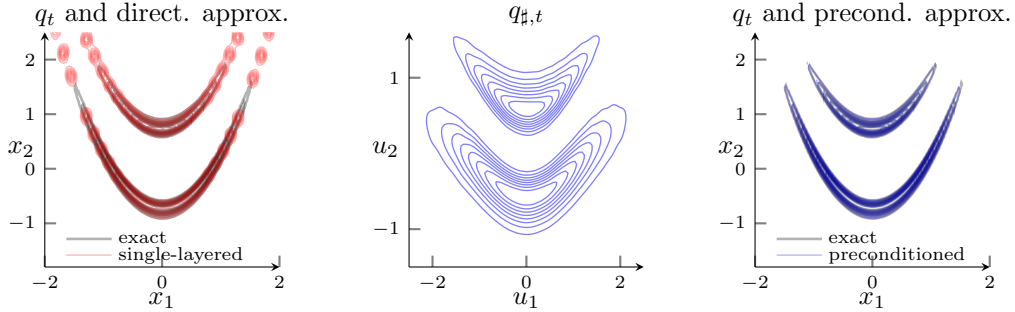


Figure 2: Left: approximation of q_t (grey contours) using a single layer of TT-based approximation (red contours), in which Fourier basis of order 30 and a TT rank 24 is used. Middle: preconditioned density using the tempering technique (cf. Section 5.3), in which the nonlinear preconditioning transform is defined by a TT with Fourier basis of order 30 and a rank 12. Right: approximation of q_t (grey contours) using the preconditioned approximation (blue contours), in which Fourier basis of order 30 and a TT rank 12 is used in the preconditioned approximation.

5.2 Gaussian bridging and linear preconditioning

We consider a Gaussian approximation to the density q_t as the bridging density, i.e., $\rho_t(\cdot) := \mathcal{N}(\cdot; \boldsymbol{\mu}_t, \boldsymbol{\Sigma}_t)$, where $\boldsymbol{\mu}_t \in \mathbb{R}^{2m+d}$ is the mean vector and $\boldsymbol{\Sigma}_t \in \mathbb{R}^{(2m+d) \times (2m+d)}$ is the covariance matrix. In each iteration, we can draw random variables from the previous marginal approximation $\hat{\pi}(\boldsymbol{\theta}, \mathbf{x}_{t-1} | \mathbf{y}_{1:t-1})$ and use one step of particle filter—e.g., a bootstrap filter—to estimate $(\boldsymbol{\mu}_t, \boldsymbol{\Sigma}_t)$ using particles. With $\rho_t(\cdot) := \mathcal{N}(\cdot; \boldsymbol{\mu}_t, \boldsymbol{\Sigma}_t)$, we compute the Cholesky factorization of $\boldsymbol{\Sigma}_t$ to obtain $\mathbf{L}_t \mathbf{L}_t^\top = \boldsymbol{\Sigma}_t$, where \mathbf{L}_t is lower-triangular. This defines a lower-triangular linear KR rearrangement $\mathcal{T}_t^l(\mathbf{x}_t, \boldsymbol{\theta}, \mathbf{x}_{t-1}) = \mathbf{L}_t[\mathbf{x}_t, \boldsymbol{\theta}, \mathbf{x}_{t-1}]^\top + \boldsymbol{\mu}_t$ that transforms $(\mathbf{X}_t, \boldsymbol{\Theta}, \mathbf{X}_{t-1}) \sim \rho_t$ into reference variables $(\mathbf{U}_t, \mathbf{U}_\theta, \mathbf{U}_{t-1})$ following a tensor-product zero mean standard Gaussian density η . The upper-triangular linear KR rearrangement can also be derived by permuting the variables.

5.3 Tempering and nonlinear preconditioning

We employ the tempering idea, e.g., Beskos et al. (2016); Gelman and Meng (1998); Herbst and Schorfheide (2019) and Kantas et al. (2014), to build an unnormalized bridging density

$$\rho_t(\mathbf{x}_t, \boldsymbol{\theta}, \mathbf{x}_{t-1}) = \hat{\pi}(\boldsymbol{\theta}, \mathbf{x}_{t-1} | \mathbf{y}_{1:t-1})^{\beta_\pi} f(\mathbf{x}_t | \mathbf{x}_{t-1}, \boldsymbol{\theta})^{\beta_f} g(\mathbf{y}_t | \mathbf{x}_t, \boldsymbol{\theta})^{\beta_g}, \quad (50)$$

with some constants $\beta_\pi, \beta_f, \beta_g \in [0, 1]$. When $\beta_\pi = \beta_f = \beta_g = 1$, it recovers the target density q_t . By choosing appropriate constants $(\beta_\pi, \beta_f, \beta_g)$ —for example, using the adaptation strategy discussed in Beskos et al. (2016) and Kantas et al. (2014)—to construct ρ_t that is less concentrate than q_t but retains some of the features of q_t . We can apply the squared approximation procedure to decompose $\sqrt{\rho_t}$ into a TT $\phi_{\rho,t}$, approximate ρ_t by

$$\hat{\rho}_t(\mathbf{x}_t, \boldsymbol{\theta}, \mathbf{x}_{t-1}) := \phi_{\rho,t}(\mathbf{x}_t, \boldsymbol{\theta}, \mathbf{x}_{t-1})^2 + \tau_{\rho,t} \lambda(\mathbf{x}_t, \boldsymbol{\theta}, \mathbf{x}_{t-1}), \quad (51)$$

with some $\tau_{\rho,t} > 0$, and derive the corresponding KR rearrangement \mathcal{R}_t such that

$$(\mathcal{R}_t)_\sharp \hat{\rho}_t(\boldsymbol{\xi}_t, \boldsymbol{\xi}_\theta, \boldsymbol{\xi}_{t-1}) \propto \text{uniform}(\boldsymbol{\xi}_t, \boldsymbol{\xi}_\theta, \boldsymbol{\xi}_{t-1}).$$

Given a diagonal map \mathcal{D} such that $\mathcal{D}_{\sharp} \eta(\xi_t, \xi_{\theta}, \xi_{t-1}) = \text{uniform}(\xi_t, \xi_{\theta}, \xi_{t-1})$, composing \mathcal{D}^{-1} and \mathcal{R}_t , we obtain $\mathcal{T}_t = \mathcal{D}^{-1} \circ \mathcal{R}_t$ such that

$$(\mathcal{T}_t)_{\sharp} \hat{\rho}_t(\mathbf{u}_t, \mathbf{u}_{\theta}, \mathbf{u}_{t-1}) \propto \eta(\mathbf{u}_t, \mathbf{u}_{\theta}, \mathbf{u}_{t-1}). \quad (52)$$

In this construction, the preconditioned target density $q_{\sharp, t}$ —which is originally defined in (44)—becomes

$$q_{\sharp, t}(\mathbf{u}_t, \mathbf{u}_{\theta}, \mathbf{u}_{t-1}) := \frac{q_t(\mathcal{T}_t^{-1}(\mathbf{u}_t, \mathbf{u}_{\theta}, \mathbf{u}_{t-1}))}{\hat{\rho}_t(\mathcal{T}_t^{-1}(\mathbf{u}_t, \mathbf{u}_{\theta}, \mathbf{u}_{t-1}))} \eta(\mathbf{u}_t, \mathbf{u}_{\theta}, \mathbf{u}_{t-1}), \quad (53)$$

where the exact bridging density ρ_t is replaced with $\hat{\rho}_t$, which is the pushforward of the reference density under the preconditioning map \mathcal{T}_t . As a consequence, the unnormalized approximate density in (49) becomes

$$\hat{\pi}(\mathbf{x}_t, \boldsymbol{\theta}, \mathbf{x}_{t-1} | \mathbf{y}_{1:t}) = \frac{\hat{\nu}_{\sharp, t}(\mathcal{T}_t(\mathbf{x}_t, \boldsymbol{\theta}, \mathbf{x}_{t-1}))}{\eta(\mathcal{T}_t(\mathbf{x}_t, \boldsymbol{\theta}, \mathbf{x}_{t-1}))} \hat{\rho}_t(\mathbf{x}_t, \boldsymbol{\theta}, \mathbf{x}_{t-1}). \quad (54)$$

5.4 Marginalization and conditional maps

After building the preconditioned approximation, we need to integrate the approximate density $\hat{\pi}(\mathbf{x}_t, \boldsymbol{\theta}, \mathbf{x}_{t-1} | \mathbf{y}_{1:t})$ over \mathbf{x}_{t-1} , so that the marginal density

$$\hat{\pi}(\mathbf{x}_t, \boldsymbol{\theta} | \mathbf{y}_{1:t}) = \int \hat{\pi}(\mathbf{x}_t, \boldsymbol{\theta}, \mathbf{x}_{t-1} | \mathbf{y}_{1:t}) d\mathbf{x}_{t-1}$$

can be used in the next iteration of Alg. 2. In addition, we also need to derive the lower and upper conditional KR rearrangements to be used in path estimation and particle filtering, respectively. We use the lower-triangular KR rearrangements \mathcal{S}_t^l and \mathcal{T}_t^l , which respectively take the form

$$\mathcal{S}_t^l(\mathbf{u}_t, \mathbf{u}_{\theta}, \mathbf{u}_{t-1}) = \begin{bmatrix} \mathcal{S}_{t,t}^l(\mathbf{u}_t) \\ \mathcal{S}_{t,\theta}^l(\mathbf{u}_{\theta} | \mathbf{u}_t) \\ \mathcal{S}_{t,t-1}^l(\mathbf{u}_{t-1} | \mathbf{u}_t, \mathbf{u}_{\theta}) \end{bmatrix} \quad \text{and} \quad \mathcal{T}_t^l(\mathbf{x}_t, \boldsymbol{\theta}, \mathbf{x}_{t-1}) = \begin{bmatrix} \mathcal{T}_{t,t}^l(\mathbf{x}_t) \\ \mathcal{T}_{t,\theta}^l(\boldsymbol{\theta} | \mathbf{x}_t) \\ \mathcal{T}_{t,t-1}^l(\mathbf{x}_{t-1} | \mathbf{x}_t, \boldsymbol{\theta}) \end{bmatrix},$$

as well as the nonlinear preconditioning defined above, to outline how to carry the marginalizations and conditional sampling.

Because the composition $\mathcal{S}_t^l \circ \mathcal{T}_t^l$ is also lower triangular, we can apply a similar derivation to that of Proposition 4 to compute the marginal density $\hat{\pi}(\mathbf{x}_t, \boldsymbol{\theta} | \mathbf{y}_{1:t})$. The necessary steps for computing $\hat{\pi}(\mathbf{x}_t, \boldsymbol{\theta} | \mathbf{y}_{1:t})$ is integrated with the preconditioned density approximation procedure, and thus we summarize them together in Alg. 5, which replace steps (b) and (c) of the sequential estimation algorithm (cf. Alg. 2).

Algorithm 5: Preconditioned replacements for steps (b) and (c) of the sequential estimation algorithm (cf. Alg. 2).

(b.1) Approximate the bridging density $\rho_t(\mathbf{x}_t, \boldsymbol{\theta}, \mathbf{x}_{t-1})$ by the TT-based approximate density $\hat{\rho}_t(\mathbf{x}_t, \boldsymbol{\theta}, \mathbf{x}_{t-1})$ defined in (51).

- (b.2) Integrate $\hat{\rho}_t(\mathbf{x}_t, \boldsymbol{\theta}, \mathbf{x}_{t-1})$ from the right variable $x_{t-1,m}$ to the left variable $x_{t,1}$ using Proposition 2 to define lower-triangular preconditioning map \mathcal{T}_t^l , the lower conditional map $\mathcal{T}_{t,t-1}^l(\mathbf{x}_{t-1}|\mathbf{x}_t, \boldsymbol{\theta})$, and the marginal density $\hat{\rho}_t(\mathbf{x}_t, \boldsymbol{\theta})$.
- (b.3) Approximate the pushforward density $q_{\sharp,t}(\mathbf{u}_t, \mathbf{u}_\theta, \mathbf{u}_{t-1})$ by the TT-based approximation $\hat{\nu}_{\sharp,t}(\mathbf{u}_t, \mathbf{u}_\theta, \mathbf{u}_{t-1})$ defined in (46).
- (c.1) Integrate the last block of $\hat{\nu}_{\sharp,t}(\mathbf{u}_t, \mathbf{u}_\theta, \mathbf{u}_{t-1})$ from the right variable $u_{t-1,m}$ to the left variable $u_{t-1,1}$ using Proposition 2 to define the marginal density $\hat{\nu}_{\sharp,t}(\mathbf{u}_t, \mathbf{u}_\theta)$ and the lower conditional map $\mathcal{S}_{t,t-1}^l(\mathbf{u}_{t-1}|\mathbf{u}_t, \mathbf{u}_\theta)$.
- (c.2) Using the lower-triangular transformation $(\mathbf{u}_t, \mathbf{u}_\theta) = (\mathcal{T}_{t,t}^l(\mathbf{x}_t), \mathcal{T}_{t,\theta}^l(\boldsymbol{\theta}|\mathbf{x}_t))$, we have the marginal density

$$\hat{\pi}(\mathbf{x}_t, \boldsymbol{\theta}|\mathbf{y}_{1:t}) = \frac{\hat{\nu}_{\sharp,t}(\mathcal{T}_{t,t}^l(\mathbf{x}_t), \mathcal{T}_{t,\theta}^l(\boldsymbol{\theta}|\mathbf{x}_t))}{\eta(\mathcal{T}_{t,t}^l(\mathbf{x}_t), \mathcal{T}_{t,\theta}^l(\boldsymbol{\theta}|\mathbf{x}_t))} \hat{\rho}_t(\mathbf{x}_t, \boldsymbol{\theta}),$$

which will be used in the next iteration of the sequential estimation.

As a byproduct, steps (b.2) and (c.1) of Alg. 5 also define the last block of the composite map $\mathcal{S}_t^l \circ \mathcal{T}_t^l$, which can be expressed as

$$\mathcal{F}_{t,t-1}^l(\mathbf{x}_{t-1}|\mathbf{x}_t, \boldsymbol{\theta}) := \mathcal{S}_{t,t-1}^l(\mathcal{T}_{t,t-1}^l(\mathbf{x}_{t-1}|\mathbf{x}_t, \boldsymbol{\theta})|\mathcal{T}_{t,t}^l(\mathbf{x}_t), \mathcal{T}_{t,\theta}^l(\boldsymbol{\theta}|\mathbf{x}_t)). \quad (55)$$

This precisely gives the lower conditional map for the path estimation (cf. Alg. 4).

6 Numerical results

We provide several numerical examples to demonstrate the efficiency of our proposed method. These include a linear Kalman filter controlled by unknown parameters, in which the posterior density of the parameters has an analytical form; a stochastic volatility model (cf. Example 1) commonly used in the literature for benchmarking sequential algorithms; and a dynamical system modelling the interaction of a predator-prey system. We also compare our method to SMC². For all the numerical examples reported here, we compute the 25%, 50%, 75% quantiles of the effective sample sizes using 40 repeated experiments.

6.1 Linear Kalman filter with unknown parameters

Setup. Our first example considers linear Kalman filter with unknown parameters, with the state and observation processes specified by

$$\begin{cases} \mathbf{X}_t - \mu &= b(\mathbf{X}_{t-1} - \mu) + a\varepsilon_t^{(x)} \\ \mathbf{Y}_t &= \mathbf{C}\mathbf{X}_t + d\varepsilon_t^{(y)} \end{cases}, \quad (56)$$

where $\varepsilon_t^{(x)}$ and $\varepsilon_t^{(y)}$ are respectively independent Gaussian distributions $\mathcal{N}(0, \mathbf{I}_m)$ and $\mathcal{N}(0, \mathbf{I}_n)$, and $\mathbf{C} \in \mathbb{R}^{n \times m}$ is the observation matrix. Here \mathbf{I}_m represents an $m \times m$ identity matrix. The prior density for the initial state \mathbf{X}_0 is given by $p(\mathbf{x}_0|\mu) := \mathcal{N}(\mathbf{x}_0; \mu\mathbf{1}, \mathbf{I}_m)$, where $\mathbf{1}$ is the

m -dimensional vector filled with ones. The parameters controlling the model are collected as $\boldsymbol{\theta} = (\mu, a, b, d)$.

Conditioned on the parameters, the joint state filtering density $p(\mathbf{x}_{0:t}|\boldsymbol{\theta}, \mathbf{y}_{1:t})$ follows a multivariable Gaussian distribution, which can be derived from the classical Kalman filter. Integrating over the states, we obtain an explicit form of the posterior parameter density $p(\boldsymbol{\theta}|\mathbf{y}_{1:t}) = \int p(\mathbf{x}_{0:t}, \boldsymbol{\theta}|\mathbf{y}_{1:t})d\mathbf{x}_{0:t}$. Although the posterior parameter density cannot be directly sampled, we can evaluate the density pointwise for any given parameter $\boldsymbol{\theta}$, and thus we can use the model in (56) to benchmark the performance of various estimation algorithms—for example, this enables us to estimate the Hellinger distance between the approximate posterior parameter density $\hat{p}(\boldsymbol{\theta}|\mathbf{y}_{1:t})$ obtained by Alg. 2 and the exact posterior parameter density $p(\boldsymbol{\theta}|\mathbf{y}_{1:t})$. For the sake of completeness, we include the derivation of the posterior parameter density $p(\boldsymbol{\theta}|\mathbf{y}_{1:t})$ in Appendix B.

In our numerical experiment, we take m and n to be three and let the total number of time steps T be 50. Additionally, we set $\mu = 0$ and fix the observation matrix \mathbf{C} to prescribed values. We impose the condition $a^2 + b^2 = 1$ to make the state process \mathbf{X}_t stationary. Thus the parameters to be estimated are reduced to $\boldsymbol{\theta} = (a, d)$. We impose a uniform prior density $p_0(\boldsymbol{\theta}) := \text{uniform}(\boldsymbol{\theta}; [0.4, 1]^2)$ on the parameters, and generate synthetic data \mathbf{Y}_t using $a = 0.8$ and $d = 0.5$ in the numerical experiments. When establishing TT approximation, we transform the parameters to an unbounded domain using the inverse distribution functions of standard Gaussian distribution to facilitate the linear preconditioning techniques in Sec. 5.2.

Comparison of Alg. 1 and 2. We start with the comparison between Alg. 1 and 2. For both algorithms, we use 5 alternating least square (ALS) iterations to construct TT decompositions. Note that using two ALS iterations is sufficient in most of the situations presented here. We use a rather large number of ALS iterations here to eliminate possible error sources in our benchmarks. The TT decomposition used here employs a piecewise Lagrange basis defined by four subintervals and polynomials with order 8. We consider maximum TT ranks $r = \{10, 20, 30\}$ in this comparison.

Following the discussion of Section 4.2, we use the relative L^1 norm, $\|\hat{\pi}_t - \pi_t\|_{L^1}/\|\pi_t\|_{L^1}$, to benchmark the accuracy of these TT-based algorithms. Note that the denominator $\|\pi_t\|_{L^1}$ is also the normalizing constant of the posterior density π_t . Fig. 3 shows the change of relative L^1 norm over time. For both algorithms, we observe that the error accumulations behave similarly and relative errors reduce with increasing TT ranks. For all TT ranks, Alg. 2 is slightly more accurate than Alg. 1 in this case. In the rest of numerical experiments, we only demonstrate the performance of Alg. 2 and its accompanying sampling algorithms.

Demonstration of Alg. 2 and debiasing. Since the non-negativity-preserving Alg. 2 is the workhorse of this paper, here we thoroughly demonstrate its accuracy and the sampling performance of the accompanying path estimation algorithm (cf. Alg. 4) with various algorithmic settings. In all experiments, we use 5 ALS iterations to construct TT decompositions and piecewise basis functions defined on four subintervals with Lagrange polynomials. We denote the degrees of freedom of the basis functions by ℓ .

In the first set of numerical experiments, we vary the degrees of freedom of the piecewise basis functions ℓ and the maximum TT-rank r to investigate their impact on the accuracy of TT-based methods. The linear preconditioning (cf. Section 5.2) is used in this case. We first fix the maximum TT-rank r to be 15 and vary $\ell = \{17, 25, 33, 41, 49\}$ by fixing the number

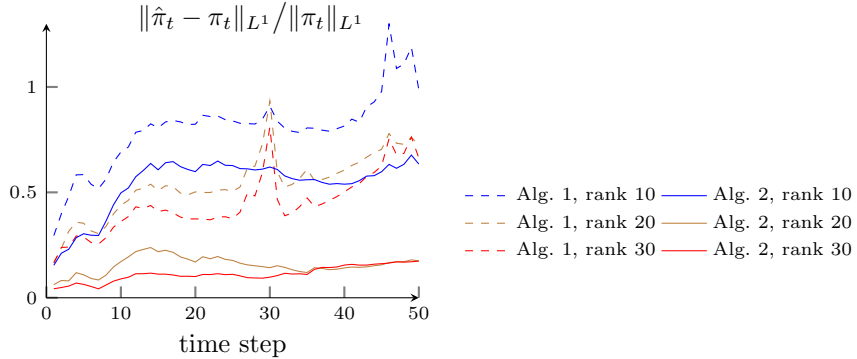


Figure 3: Linear Kalman filter with unknown parameters. The relative L^1 errors of approximations built by Alg. 1 and 2.

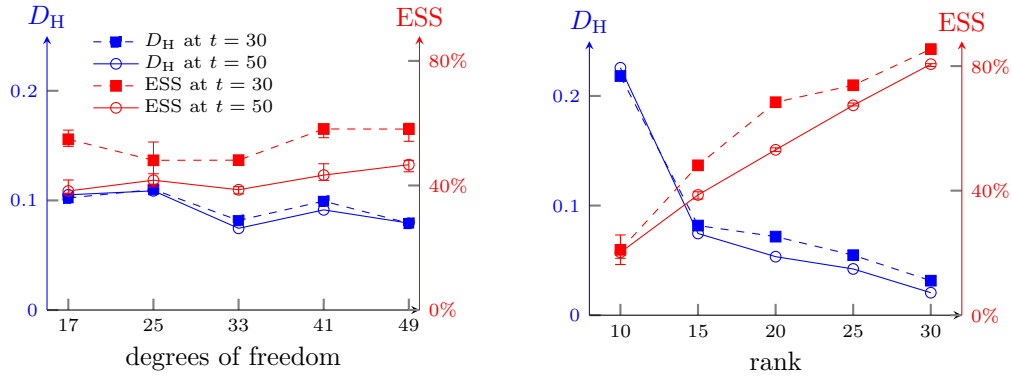


Figure 4: Linear Kalman filter with unknown parameters. The Hellinger errors (blue lines) of the TT-approximate posterior parameter density and the ESS (red lines) for the joint posterior at time $t = \{30, 50\}$. Left: changing the degrees of freedom of the basis function with a fixed maximum TT rank $r = 15$. Right: changing the maximum TT rank $r = 15$ with fixed degrees of freedom of the basis function $\ell = 33$.

of subintervals to be four and increasing the order of the Lagrange polynomials. For each ℓ , we run Alg. 2 for t up to 50 and apply the path estimation (Alg. 4) using $N = 1000$ sample paths at $t \in \{30, 50\}$. For each of the approximate posterior parameter densities, we report its Hellinger error and the effective sample size (ESS)—for the joint density $p(\boldsymbol{\theta}, \mathbf{x}_{0:t} | \mathbf{y}_{1:t})$ —at $t \in \{30, 50\}$ in the left plot of Fig. 4. Here we observe that increasing the degrees of freedom of the basis functions only marginally improves the accuracy. Then we fix the degrees of freedom ℓ to be 33 with order-eight Lagrange polynomials on four subintervals, and vary the maximum TT-rank $r = \{10, 15, 20, 25, 30\}$. The resulting Hellinger distances and ESSs are shown in the right plot of Fig. 4. In this case, we observe a significant error reduction with increasing TT-rank.

In the second set of numerical experiments, we demonstrate the impact of preconditioning techniques. Here we consider two approximation ansatzes with $(\ell, r) = (33, 15)$ and $(\ell, r) = (33, 30)$ using the linear preconditioning (cf. Section 5.2) and another ansatz $(\ell, r) = (33, 15)$ using the nonlinear preconditioning (cf. Section 5.3). For the nonlinear

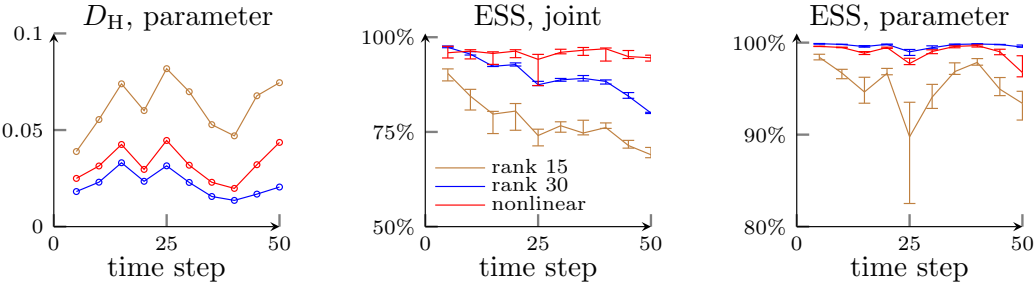


Figure 5: Linear Kalman filter with unknown parameters. Left: the Hellinger error of the approximate posterior parameter density $\hat{p}(\theta|y_{1:t})$ at different time. Middle: the ESS of the path estimation (cf. Alg. 4) for sampling the joint posterior $p(\theta, x_{0:t}|y_{1:t})$ versus time. Right: the ESS for sampling the posterior parameter density $p(\theta|y_{1:t})$ versus time.

preconditioning, we use a standard multivariate Gaussian for the reference density η and $\beta_\pi = \beta_f = \beta_g = 0.4$ to construct the bridging density. For each of $t \in \{1, \dots, 50\}$, we report the Hellinger error of the approximate posterior parameter density, the ESS of path estimation (Alg. 4) for the joint density, and the ESS of the approximate posterior parameter density. The results are shown in Fig. 5. In the linear preconditioning case, we observe that the approximation ansatz $(\ell, r) = (33, 30)$ performs better than the approximation ansatz $(\ell, r) = (33, 15)$ for all time steps, which is expected. We also observe that the performance of the nonlinear preconditioning technique using the approximation ansatz $(\ell, r) = (33, 15)$ is comparable with that of the linear preconditioning with a higher-rank approximation ansatz $(\ell, r) = (33, 30)$. For both $(\ell, r) = (33, 15)$ using the nonlinear preconditioning and $(\ell, r) = (33, 30)$ using the linear preconditioning, the Hellinger errors remain below 0.05 for all time steps, while the ESSs for the joint densities and the marginal parameter densities are respectively around 80% and 99% after 50 time steps. These results provide strong evidence of the reliability of the TT-based sequential estimation methods.

Comparison with SMC². We compare Alg. 2 with $(\ell, r) = (33, 30)$ and $(\ell, r) = (33, 15)$ to the SMC² method. We consider two setups for the SMC² method. One uses a particle size $N_\theta = 500$ for the parameters and another one uses an increased particle size $N_\theta = 5000$. In all numerical experiments, the particle size for the states is initially set to $N_x = 100$ and adaptively increased so that the acceptance rate of the parameter particles remains a relatively high level (Chopin et al., 2013). In our setup, the computational cost of running SMC² with $(N_\theta, N_x) = (500, 100)$ is about the same as running Alg. 2 with $(\ell, r) = (33, 30)$. Both take roughly 10 minutes using a 3.20 GHz Intel i7-8700 CPU. In Fig. 6, we present contours of the posterior parameter densities and one-dimensional marginals at times $t \in \{10, 30, 50\}$ estimated using various algorithms. For SMC², we follow the setup of Chopin et al. (2013) to run five independent batches of particles, and then apply the kernel density estimation (KDE) method (Silverman, 1986; Peter D, 1985) to estimate the joint density using the union of the five batches and the one-dimensional parameter marginal density for each batch. Both TT-based setups perform better than the SMC²-based setups.

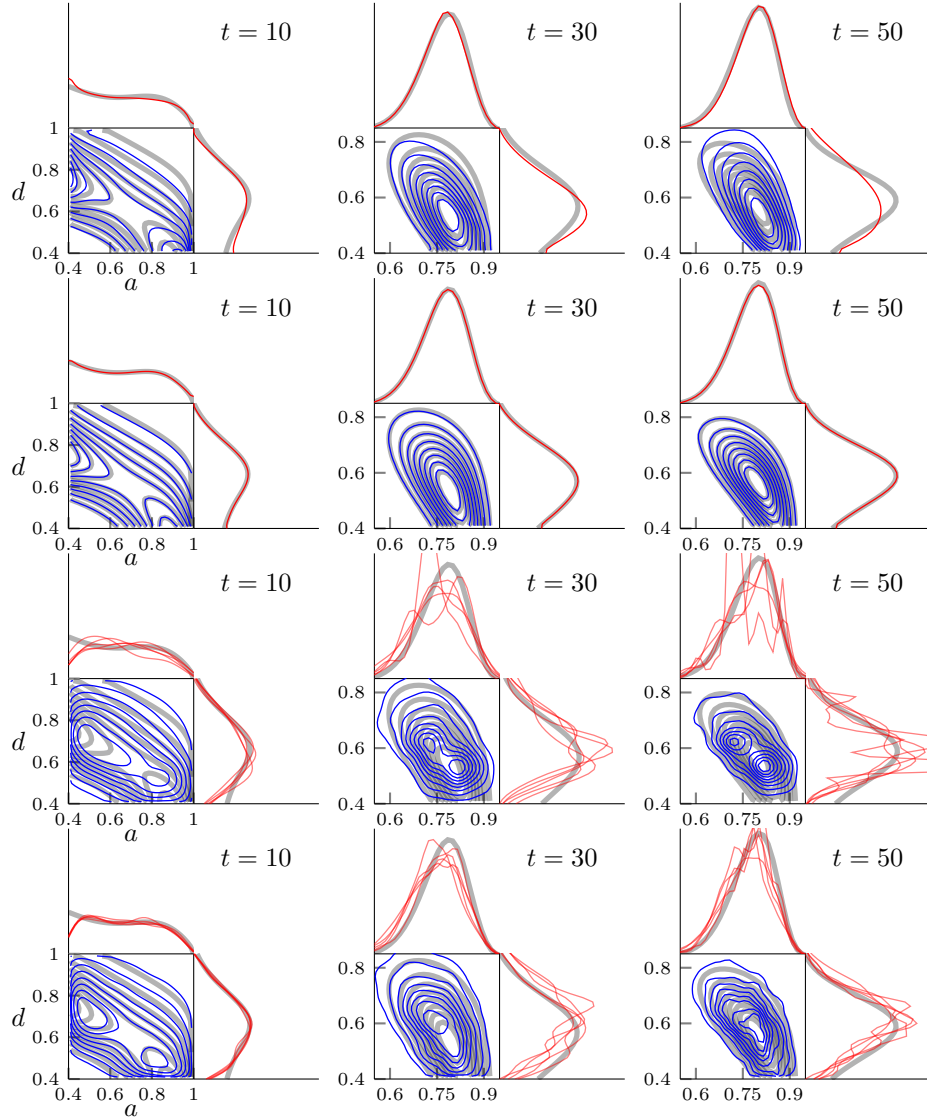


Figure 6: Linear Kalman filter with unknown parameters. The contours of posterior densities of $\boldsymbol{\theta} = (a, d)$ at different times. From the top row to the bottom row, blue lines are results obtained by Alg. 2 with $(\ell, r) = (33, 15)$, Alg. 2 with $(\ell, r) = (33, 30)$, SMC² with 500 particles, and SMC² with 5000 particles, respectively. The marginal densities are shown by red curves on each side. The analytical solutions are plotted as thick grey curves at the background. For SMC², the marginal densities are results obtained from 5 batches, whereas the contours are results obtained by putting all batches together.

6.2 Stochastic volatility

Our second example uses the stochastic volatility model defined in Example 1. We fix $\sigma = 1$ and aim to estimate parameters $\boldsymbol{\theta} = (\gamma, \beta)$. We consider the sequential estimation problems for $T = 1000$ steps. Here $\gamma = 0.6$ and $\beta = 0.4$ are used to generate synthetic data. We set the prior density for the initial state to be $p(\mathbf{x}|\boldsymbol{\theta}) := \mathcal{N}(\mathbf{x}; 0, \sigma^2/(1 + \gamma^2))$

and the prior density for the parameters to be $p_0(\boldsymbol{\theta}) := \text{uniform}(\boldsymbol{\theta}; [0.1, 0.9]^2)$. Since the analytical marginal densities are no longer available in this example, we can only evaluate the 1002-dimensional joint posterior density for the parameters and all states $(\boldsymbol{\theta}, \mathbf{x}_{0:1000})$ and estimate the corresponding ESS as a benchmark on the approximation errors.

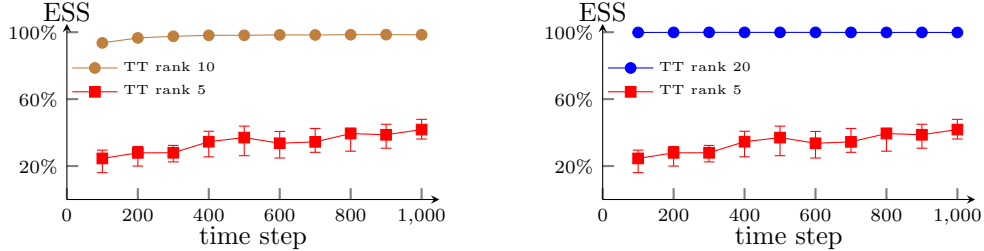


Figure 7: Stochastic volatility model. ESS for the joint posterior density at different times, computed using different maximum TT ranks $r = \{5, 10, 20\}$.

Similar to the linear Kalman filter case, we use the piecewise Lagrange polynomial with degrees of freedom $\ell = 33$ as the basis function, the linear preconditioning, and 5 ALS iterations for building TT decomposition in Alg. 2. The accompanying path estimation algorithm (cf. Alg. 4) is used to generate weighted samples from the resulting TT-based approximations. We set the maximum TT-rank to be $r \in \{5, 10, 20\}$ and show the change of ESS versus time in Fig. 7. We observe that with $r = 5$, the TT-based approximation yields a reliable result with ESS above 20% even after 1000 steps, while with $r = 10$ it provides nearly 100% ESS in almost all time steps. Figure 8 presents the trajectories of the states estimated from the approximate posterior state path density $\hat{p}(\mathbf{x}_{0:1000} | \mathbf{y}_{1:1000})$ using rank $r = 10$. We observe the true states are well followed by the trajectories estimated from the approximations. In Fig. 9, we also show the approximate filtering densities of the parameter γ from the TT-based approximations, $\hat{p}(\gamma | \mathbf{y}_{1:t})$. We observe that the densities get concentrated around the true value $\gamma = 0.6$ (for generating the data) with an increasing amount of data observed over time.

Next, we compare the TT-based method with $r = 10$ to SMC² with 5 batches and each batch with $N_\theta = 1000$ parameter particles and initially $N_x = 100$ state particles. Fig. 10 shows the contours and marginals of the parameter posterior densities at $t = \{400, 700, 1000\}$ obtained by the TT-based method and SMC². Both methods yield densities that concentrate around the true values of the parameters used to generate the data, i.e., $(\gamma, \beta) = (0.6, 0.4)$. However, the computation time of the TT-based method is about one hour using a 3.20 GHz Intel i7-8700 CPU, while that for one batch of SMC² method is over eight hours.

6.3 Predator and prey model

We then consider the predator and prey model, which is a time-invariant dynamical system in the form of

$$\begin{cases} \frac{dP}{dt} = rP\left(1 - \frac{P}{K}\right) - s\left(\frac{sPQ}{a+P}\right) \\ \frac{dQ}{dt} = u\left(\frac{PQ}{a+P} - vQ\right) \end{cases}, \quad (57)$$

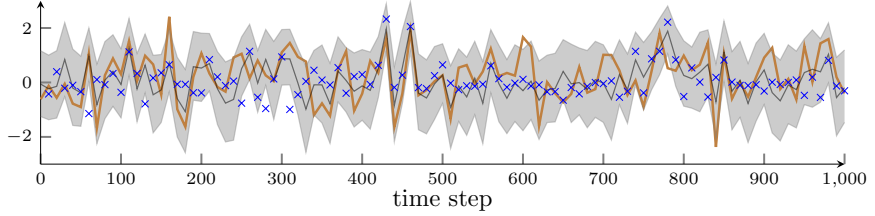


Figure 8: Stochastic volatility model. The thick brown line represents the path of the true state and crosses are the observations. Estimated using the approximate posterior state path density $\hat{p}(\mathbf{x}_{0:1000}|\mathbf{y}_{1:1000})$ defined in (31) with a maximum TT rank $r = 10$, the black line and the shaded region represent the median path and the credible interval bounded between 5% and 95% percentiles, respectively.

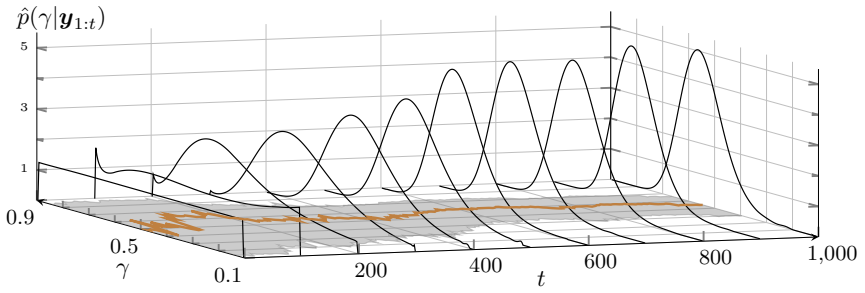


Figure 9: Stochastic volatility model. The brown line and the shaded region in the (t, γ) horizontal plane show the evolution of the median and the credible interval of posterior parameters bounded between 5% and 95% percentiles over time. The density profiles in the vertical axis show the approximate posterior parameter density $\hat{p}(\gamma|\mathbf{y}_{1:t})$ at different times.

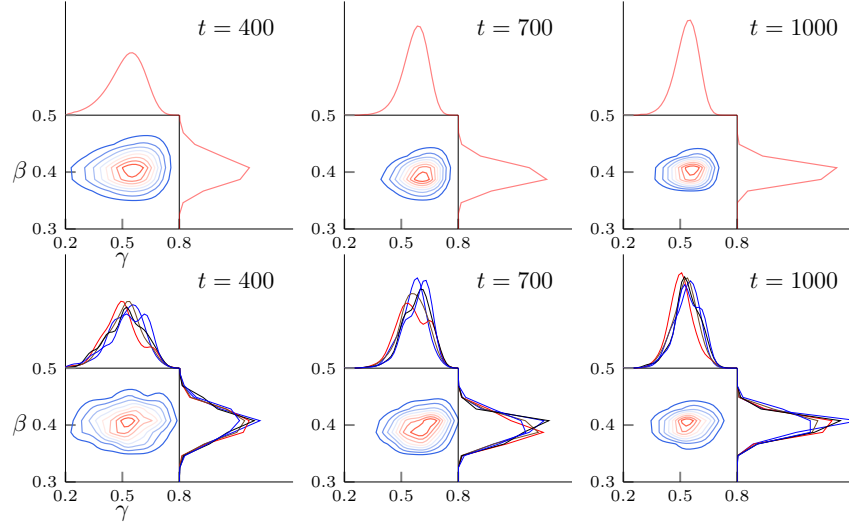


Figure 10: Stochastic volatility model. The contours of posterior densities of $\boldsymbol{\theta} = (\gamma, \beta)$ at different times. The top and bottom rows show results obtained by Alg. 2 and SMC² respectively. The marginal densities are shown on each side. For SMC², the marginal densities shown are results obtained from 5 batches with 1000 particles in each batch, whereas the contours are results obtained by putting all batches together.

where P and Q denote the population of prey and the population of predator, respectively. There are size parameters, $\boldsymbol{\theta} = (r, K, a, s, u, v)$, that control the behaviour of the system. To formulate the state space model, we represent the states P and Q as $\mathbf{x} = (P, Q)$. This way, the dynamical system in (57) can be equivalently expressed as

$$\frac{d\mathbf{x}}{dt} = G(\mathbf{x}; \boldsymbol{\theta}),$$

where $G(\mathbf{x}; \boldsymbol{\theta})$ is defined by the right hand side of (57). We discretize the dynamical system at discrete times $t = k\Delta t$, where $\Delta t = 4$, and perturb the states using a Gaussian noise $\varepsilon_k^{(x)} \sim \mathcal{N}(\mathbf{0}, 25\mathbf{I}_2)$. This way, conditioned on the state \mathbf{X}_{k-1} at time $(k-1)\Delta t$, the state \mathbf{X}_k at time $k\Delta t$ is given by

$$\mathbf{X}_k = \mathbf{X}_{k-1} + \int_{(k-1)\Delta t}^{k\Delta t} G(\mathbf{x}(t); \boldsymbol{\theta}) dt + \varepsilon_k^{(x)},$$

where $\mathbf{x}(t) = \mathbf{X}_{k-1}$ for $t = (k-1)\Delta t$ in the above time integration. We use the explicit Runge–Kutta (4, 5) formula with adaptive time stepping (`ode45` of MATLAB) to numerically solve the above time integration problem. We observe \mathbf{x} at the same sequence of discrete times, and the observations are perturbed by Gaussian noise $\varepsilon_k^{(y)} \sim \mathcal{N}(\mathbf{0}, \mathbf{I}_2)$. This defines the observation process

$$\mathbf{Y}_k = \mathbf{X}_k + \varepsilon_k^{(y)}.$$

We generate synthetic observations using $\boldsymbol{\theta} = (0.6, 114, 25, 0.3, 0.5, 0.5)$ and $\mathbf{x}_0 = [50, 5]^\top$ up to the terminal time $T = 10$. We impose a uniform prior on the parameters, $p(\boldsymbol{\theta}) := \text{uniform}(\boldsymbol{\theta}; [\mathbf{a}, \mathbf{b}])$, where $[\mathbf{a}, \mathbf{b}] \equiv [a_1, b_1] \times \cdots \times [a_6, b_6]$ is a hypercube defined by $\mathbf{a} = (0.1, 110, 20, 0.1, 0, 0)$ and $\mathbf{b} = (1.1, 130, 30, 1.1, 1, 1)$. We further impose a Gaussian prior on the initial states $p(\mathbf{x}_0) := \mathcal{N}(\mathbf{x}_0; \boldsymbol{\mu}_0, \mathbf{I}_2)$ where $\boldsymbol{\mu}_0 = (50, 5)$.

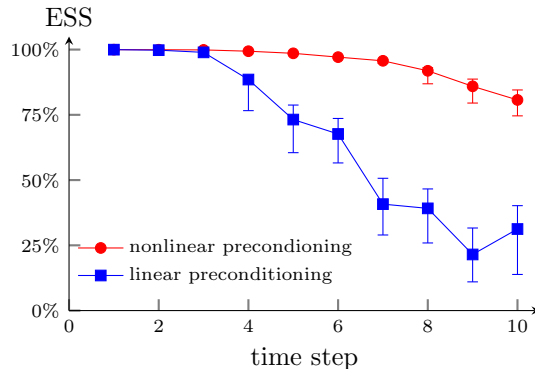


Figure 11: Predator and prey model. ESS for joint posterior density at different times, computed using different preconditioning techniques.

We first employ Alg. 2 with the linear preconditioning, the piecewise Lagrange polynomial with degrees of freedom $\ell = 33$, a maximum TT rank $r = 30$, and an ALS iterations of 5. The accompanying path estimation algorithm (cf. Alg. 4) is used to generate weighted samples from the resulting TT-based approximations. In Fig. 11, the ESS for the joint

posterior density of the parameters and all states are represented by square markers. In this case, the ESS decreases rapidly. Rather than increasing the TT rank to enhance its approximation power, we keep the same TT rank and apply the nonlinear preconditioning. Here we use the bridging density (50) with $\beta_\pi = \beta_f = \beta_g = 0.05$. With the nonlinear preconditioning, the ESSs are shown as circles in Fig. 11. We observe that the nonlinear preconditioning significantly increases the ESS, where it remains at about 80% after 10 steps. In Fig. 12, we also present the trajectories of the states estimated from the approximate posterior state path density $\hat{p}(\mathbf{x}_{0:10}|\mathbf{y}_{1:10})$ with the true trajectories. The curves between the two adjacent states \mathbf{x}_{k-1} and \mathbf{x}_k are the solution of the dynamical system (57) with initial condition $\mathbf{x} = \mathbf{x}_{k-1}$.

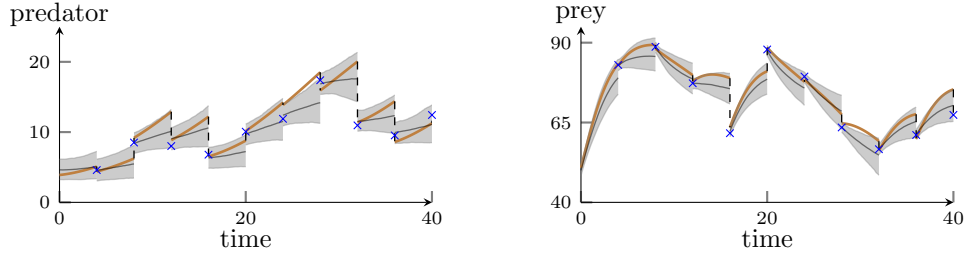


Figure 12: Predator and prey model. The thick brown curves are the true states, the dashed lines indicate the error perturbation at discrete times, crosses are the observations. The black curves represent the median posterior state path obtained by the approximate density $\hat{p}(\mathbf{x}_{0:10}|\mathbf{y}_{1:10})$, the shaded region is the credible interval bounded between 5% and 95% percentiles of the approximate smoothing densities.

7 Conclusion and further extensions

We present new TT-based methods to sequentially learn the posterior distributions of states and parameters of state-space models. Our main innovation is the recursive approximation of posterior densities using TT rather than relying on (weighted) particle representations. Using the square-root approximation technique (cf. Section 3), we derive conditional KR rearrangements that map reference random variables to the approximated posterior random variables. As a result, this defines the particle filtering, path estimation and particle smoothing algorithms accompanying the recursive TT-based approximations.

This work opens the door to many future research directions. For example, one can integrate our TT-based methods into SMC methods (Chopin et al., 2013; Crisan and Miguez, 2018), in which TT-based methods can potentially provide more efficient particle filters and MCMC proposal kernels for SMC. The KR rearrangements offered by our methods also open the door to integrating other structured particle sets—for instance, quasi Monte Carlo points (see Dick et al. (2013) and references therein)—into sequential learning algorithms to improve the rate of convergence of estimators. This integration can significantly complement the Hilbert space-filling curve technique used by the sequential quasi Monte Carlo method (Gerber and Chopin, 2015).

Further research is needed to understand the rank structure of TT decompositions in state-space models—particularly on the impact of the Markov property—which may provide

a posteriori error bounds to certify the algorithms presented here. The function approximation perspective of the work presented here is not limited to the TT decomposition. Other function approximation methods based on separable bases—for example, Gaussian processes and radial basis functions (Wendland, 2004; Williams and Rasmussen, 2006) with product-form kernels, multivariate wavelet and Fourier bases (Daubechies, 1992; de Boor et al., 1993; DeVore and Popov, 1988; Mallat, 1989), and sparse grids and spectral polynomials (Bungartz and Griebel, 2004; Shen et al., 2011; Xiu and Karniadakis, 2002)—can also be used to approximate posterior densities and compute their marginal densities. See Cui et al. (2023) for the preliminary investigations in stationary inference problems. This offers a pathway to designing problem-specific function approximation methods for sequential learning. For instance, state transition processes governed by certain partial differential equations may yield a hyperbolic-cross structure (Düng et al., 2018) suitable for sparse spectral polynomials.

Dimension scalability is a limitation of the TT decomposition and general transport-map methods. Although the complexity of building the TT decomposition can be dimension independent for functions equipped with rapid decaying weights (Griebel and Harbrecht, 2023)—which is the case for many high- or infinite-dimensional problems (Stuart, 2010)—it is still computationally prohibitive to operate with the apparent state and parameter dimensions for very high-dimensional systems such as weather forecasts. A possibility of reducing the number of variables in the approximation problem is to use the conditional Gaussian structure of certain state-space models (Chen et al., 2022, 2018; Chen and Majda, 2018) to marginalize high-dimensional conditional Gaussian variables analytically. Then, one only needs to apply TT-based approximations to the rest of the non-Gaussian variables. For a broader range of state-space models, there may exist approximate conditional Gaussian structures and similar structures that allow for analytical marginalization. In ongoing work, we are extending likelihood-informed subspace methods (Cui et al., 2014; Cui and Tong, 2022; Zahm et al., 2022) to state-space models to identify these intrinsic structures.

Acknowledgments

We would like to thank Sergey Dolgov, Rob Scheichl and Olivier Zahm for many fruitful discussions about the tensor-train and sparse polynomial methods. This work was supported in part by the Australian Research Council under the grant DP210103092.

Appendix A. f -divergence of marginal random variables

Commonly used statistical divergences such as Kullback–Leibler divergence, total variation distance and squared Hellinger distance are instances of the f -divergence. Given a convex function $f(\cdot)$, the f -divergence is defined as

$$D_f(p\|q) = \int f\left(\frac{p(\mathbf{x})}{q(\mathbf{x})}\right)q(\mathbf{x})d\mathbf{x}.$$

The following lemma bounds the f -divergence of marginal random variables by the corresponding f -divergence of joint random variables.

Lemma 14 Let $p_1(\mathbf{x}_1, \mathbf{x}_2)$ and $p_2(\mathbf{x}_1, \mathbf{x}_2)$ be two joint densities and $\bar{p}_1(\mathbf{x}_1)$ and $\bar{p}_2(\mathbf{x}_1)$ be the marginal densities of p_1 and p_2 , respectively. The f -divergence of \bar{p}_1 from \bar{p}_2 is bounded from above by that of p_1 from p_2 , i.e., $D_f(\bar{p}_1\|\bar{p}_2) \leq D_f(p_1\|p_2)$.

Proof Since the function f is convex, applying Jensen's inequality, we have

$$\begin{aligned} D_f(p_1\|p_2) &= \mathbb{E}_{p_2(\mathbf{x}_1, \mathbf{x}_2)} \left[f\left(\frac{p_1(\mathbf{X}_1, \mathbf{X}_2)}{p_2(\mathbf{X}_1, \mathbf{X}_2)}\right) \right] \\ &= \int \int \left(f\left(\frac{p_1(\mathbf{x}_1, \mathbf{x}_2)}{p_2(\mathbf{x}_1, \mathbf{x}_2)}\right) \frac{p_2(\mathbf{x}_1, \mathbf{x}_2)}{\bar{p}_2(\mathbf{x}_1)} d\mathbf{x}_2 \right) \bar{p}_2(\mathbf{x}_1) d\mathbf{x}_1 \\ &\geq \int f\left(\int \frac{p_1(\mathbf{x}_1, \mathbf{x}_2)}{p_2(\mathbf{x}_1, \mathbf{x}_2)} \frac{p_2(\mathbf{x}_1, \mathbf{x}_2)}{\bar{p}_2(\mathbf{x}_1)} d\mathbf{x}_2 \right) \bar{p}_2(\mathbf{x}_1) d\mathbf{x}_1 \\ &= \int f\left(\int \frac{p_1(\mathbf{x}_1, \mathbf{x}_2)}{\bar{p}_2(\mathbf{x}_1)} d\mathbf{x}_2 \right) \bar{p}_2(\mathbf{x}_1) d\mathbf{x}_1 \\ &= \int f\left(\frac{\bar{p}_1(\mathbf{x}_1)}{\bar{p}_2(\mathbf{x}_1)}\right) \bar{p}_2(\mathbf{x}_1) d\mathbf{x}_1 = D_f(\bar{p}_1\|\bar{p}_2), \end{aligned}$$

which concludes the proof. ■

When the densities are only known up to some constants, the L^2 distance between the square root of the unnormalized marginal densities is also bounded by that of the unnormalized joint densities. This is shown in the following lemma.

Lemma 15 Let $\pi_1(\mathbf{x}_1, \mathbf{x}_2)$ and $\pi_2(\mathbf{x}_1, \mathbf{x}_2)$ be two unnormalized densities and $\bar{\pi}_1(\mathbf{x}_1) = \int \pi_1(\mathbf{x}_1, \mathbf{x}_2) d\mathbf{x}_2$ and $\bar{\pi}_2(\mathbf{x}_1) = \int \pi_2(\mathbf{x}_1, \mathbf{x}_2) d\mathbf{x}_2$ are their corresponding marginal densities. The L^2 distance between $\sqrt{\bar{\pi}_1}$ and $\sqrt{\bar{\pi}_2}$ is bounded from above by the L^2 distance between $\sqrt{\pi_1}$ and $\sqrt{\pi_2}$, i.e., $\|\sqrt{\bar{\pi}_1} - \sqrt{\bar{\pi}_2}\|_{L^2} \leq \|\sqrt{\pi_1} - \sqrt{\pi_2}\|_{L^2}$.

Proof The L^2 distance between $\sqrt{\pi_1}$ and $\sqrt{\pi_2}$ can be expressed as

$$\begin{aligned} \|\sqrt{\pi_1} - \sqrt{\pi_2}\|_{L^2}^2 &= \int \int (\sqrt{\pi_1(\mathbf{x}_1, \mathbf{x}_2)} - \sqrt{\pi_2(\mathbf{x}_1, \mathbf{x}_2)})^2 d\mathbf{x}_1 d\mathbf{x}_2 \\ &= \int \int \left(\sqrt{\frac{\pi_1(\mathbf{x}_1, \mathbf{x}_2)}{\pi_2(\mathbf{x}_1, \mathbf{x}_2)}} - 1 \right)^2 \pi_2(\mathbf{x}_1, \mathbf{x}_2) d\mathbf{x}_1 d\mathbf{x}_2 \\ &= \int \int \left(\sqrt{\frac{\pi_1(\mathbf{x}_1, \mathbf{x}_2)}{\pi_2(\mathbf{x}_1, \mathbf{x}_2)}} - 1 \right)^2 \frac{\pi_2(\mathbf{x}_1, \mathbf{x}_2)}{\bar{\pi}_2(\mathbf{x}_1)} d\mathbf{x}_2 \bar{\pi}_2(\mathbf{x}_1) d\mathbf{x}_1. \end{aligned}$$

Since $f(r) = (\sqrt{r} - 1)^2, r \geq 0$ is a convex function, applying Jensen's inequality to the inner integral over $d\mathbf{x}_2$, the rest of the proof follows the same steps of Lemma 14. ■

Lemma 15 is useful to establish the error between two unnormalized marginal densities given that between the joint densities. Similar results can also be obtained for L^1 distance, which is analogous to the total variation distance for normalized densities. However, Lemma 15 implicitly assumes that both unnormalized joint densities are non-negative by construction. The following lemma gives a similar result under the L^1 distance, but does not restrict the approximate density to be non-negative.

Lemma 16 Let $\pi_1(\mathbf{x}_1, \mathbf{x}_2)$ be an unnormalized density and $\bar{\pi}_1(\mathbf{x}_1) = \int \pi_1(\mathbf{x}_1, \mathbf{x}_2) d\mathbf{x}_2$ be the corresponding marginal density. Suppose $\pi_1(\mathbf{x}_1, \mathbf{x}_2)$ has an approximation $\pi_2(\mathbf{x}_1, \mathbf{x}_2)$, which does not preserve the non-negativity, and let $\bar{\pi}_2(\mathbf{x}_1) = \int \pi_2(\mathbf{x}_1, \mathbf{x}_2) d\mathbf{x}_2$ be the corresponding marginal density. The L^1 distance between $\bar{\pi}_1$ and $\bar{\pi}_2$ is bounded from above by that between π_1 and π_2 , i.e., $\|\bar{\pi}_1 - \bar{\pi}_2\|_{L_1} \leq \|\pi_1 - \pi_2\|_{L_1}$.

Proof The L^1 distance between π_1 and π_2 can be expressed as

$$\begin{aligned} \|\pi_1 - \pi_2\|_{L_1} &= \int \int |\pi_1(\mathbf{x}_1, \mathbf{x}_2) - \pi_2(\mathbf{x}_1, \mathbf{x}_2)| d\mathbf{x}_1 d\mathbf{x}_2 \\ &= \int \int \left| \frac{\pi_2(\mathbf{x}_1, \mathbf{x}_2)}{\pi_1(\mathbf{x}_1, \mathbf{x}_2)} - 1 \right| \pi_1(\mathbf{x}_1, \mathbf{x}_2) d\mathbf{x}_1 d\mathbf{x}_2 \\ &= \int \int \left| \frac{\pi_2(\mathbf{x}_1, \mathbf{x}_2)}{\pi_1(\mathbf{x}_1, \mathbf{x}_2)} - 1 \right| \frac{\pi_1(\mathbf{x}_1, \mathbf{x}_2)}{\bar{\pi}_1(\mathbf{x}_1)} d\mathbf{x}_2 \bar{\pi}_1(\mathbf{x}_1) d\mathbf{x}_1. \end{aligned}$$

Since $f(r) = |r - 1|$ is a convex function, applying Jensen's inequality to the inner integral over $d\mathbf{x}_2$, the rest of the proof follows the same steps of Lemma 14. \blacksquare

Appendix B. Posterior densities of the linear Kalman filter with unknown parameters

We recall that the linear Kalman filter specifies the state and observation processes as

$$\begin{cases} \mathbf{X}_t - \mu = b(\mathbf{X}_{t-1} - \mu) + a \varepsilon_{t-1}^{(x)} \\ \mathbf{Y}_t = \mathbf{C} \mathbf{X}_t + d \varepsilon_t^{(y)} \end{cases}, \quad (58)$$

where $\varepsilon_t^{(x)}$ and $\varepsilon_t^{(y)}$ are respectively independent Gaussian distributions $\mathcal{N}(0, \mathbf{I}_m)$ and $\mathcal{N}(0, \mathbf{I}_n)$, and $\mathbf{C} \in \mathbb{R}^{n \times m}$ is the observation matrix. Here \mathbf{I}_m represents an $m \times m$ identity matrix. The prior density for the initial state \mathbf{X}_0 is given by $p(\mathbf{x}_0 | \mu) := \mathcal{N}(\mathbf{x}_0; \mu \mathbf{1}_m, \mathbf{I}_m)$, where $\mathbf{1}_m$ is the m -dimensional vector filled with ones. Without loss of generality, we set μ to be zero to simplify notation used in the derivation. This way, the parameters controlling the model are collected as $\boldsymbol{\theta} = (a, b, d)$. It is well known that the filtering density $(\mathbf{X}_t | \boldsymbol{\Theta} = \boldsymbol{\theta}, \mathbf{Y}_{1:t} = \mathbf{y}_{1:t})$ and the smoothing density $(\mathbf{X}_k | \boldsymbol{\Theta} = \boldsymbol{\theta}, \mathbf{Y}_{1:t} = \mathbf{y}_{1:t})$ for any $k < t$ are Gaussian conditioned on $\boldsymbol{\Theta} = \boldsymbol{\theta}$. See Särkkä (2013) and reference therein for details. Using this property, here we derive the analytical form of the posterior parameter density $p(\boldsymbol{\theta} | \mathbf{y}_{1:t})$.

As a starting point, we collect all the quantities from time 0 to t in vectorized forms,

$$\begin{aligned} \bar{\mathbf{X}} &= [\mathbf{X}_0; \dots; \mathbf{X}_t] \in \mathbb{R}^{m(t+1)}, \\ \bar{\mathbf{Y}} &= [\mathbf{Y}_1; \dots; \mathbf{Y}_t] \in \mathbb{R}^{nt}, \\ \bar{\varepsilon}^{(x)} &= [\varepsilon_0^{(x)}; \dots; \varepsilon_t^{(x)}] \in \mathbb{R}^{m(t+1)}, \\ \bar{\varepsilon}^{(y)} &= [\varepsilon_1^{(y)}; \dots; \varepsilon_t^{(y)}] \in \mathbb{R}^{nt}. \end{aligned}$$

Corresponding to the collected states \mathbf{X} and collected observations \mathbf{Y} , we define the joint state transition matrix $\mathbf{A}_{\boldsymbol{\theta}} \in \mathbb{R}^{m(t+1) \times m(t+1)}$ and the joint observation matrix $\mathbf{H} \in \mathbb{R}^{nt \times m(t+1)}$

as

$$\mathbf{A}_\theta = \begin{bmatrix} a \mathbf{I}_m & & & & \\ -b \mathbf{I}_m & \mathbf{I}_m & & & \\ & -b \mathbf{I}_m & \mathbf{I}_m & & \\ & & \ddots & \ddots & & \\ & & & -b \mathbf{I}_m & \mathbf{I}_m \end{bmatrix} \quad \text{and} \quad \mathbf{H} = \begin{bmatrix} 0 & \mathbf{C} & & & \\ & 0 & \mathbf{C} & & \\ & & 0 & \mathbf{C} & \\ & & & \ddots & \ddots \\ & & & & 0 & \mathbf{C} \end{bmatrix},$$

respectively, where $\mathbf{0}$ denotes a matrix of size $n \times m$ filled with zeros. Using this notation, the state and observation processes defined in (58) can be equivalently expressed as

$$\bar{\mathbf{X}} = a \mathbf{A}_\theta^{-1} \bar{\varepsilon}^{(x)}, \quad \bar{\mathbf{Y}} = \mathbf{H} \bar{\mathbf{X}} + d \bar{\varepsilon}^{(y)}.$$

The joint posterior density for the state path $\mathbf{X}_{0:t} \equiv \bar{\mathbf{X}}$ and the parameters Θ takes the form

$$p(\bar{\mathbf{x}}, \theta | \bar{\mathbf{y}}) = \frac{1}{p(\bar{\mathbf{y}})} p(\bar{\mathbf{y}} | \bar{\mathbf{x}}, \theta) p(\bar{\mathbf{x}} | \theta) p(\theta). \quad (59)$$

Our goal is to derive the posterior parameter density

$$p(\theta | \bar{\mathbf{y}}) = \int p(\bar{\mathbf{x}}, \theta | \bar{\mathbf{y}}) d\bar{\mathbf{x}} = \frac{1}{p(\bar{\mathbf{y}})} p(\theta) p(\bar{\mathbf{y}} | \theta), \quad (60)$$

where $p(\bar{\mathbf{y}} | \theta)$ is the marginal likelihood defined as

$$p(\bar{\mathbf{y}} | \theta) = \int p(\bar{\mathbf{y}} | \bar{\mathbf{x}}, \theta) p(\bar{\mathbf{x}} | \theta) p(\theta) d\bar{\mathbf{x}}. \quad (61)$$

Conditioned on the parameters $\Theta = \theta$, the prior density of the state path $\bar{\mathbf{X}}$ is defined by the state evaluation process, which takes the form

$$(\mathbf{X}_{0:t} | \Theta = \theta) \equiv (\bar{\mathbf{X}} | \Theta = \theta) \sim p(\bar{\mathbf{x}} | \theta) := \mathcal{N}(\bar{\mathbf{x}}; \mathbf{0}, a^2 \mathbf{A}_\theta^{-1} \mathbf{A}_\theta^{-\top}).$$

Similarly, given θ and $\bar{\mathbf{x}}$, the collected observations $\bar{\mathbf{Y}}$ follow the conditional density

$$(\bar{\mathbf{Y}} | \Theta = \theta, \bar{\mathbf{X}} = \bar{\mathbf{x}}) \sim p(\bar{\mathbf{y}} | \bar{\mathbf{x}}, \theta) = \mathcal{N}(\bar{\mathbf{y}}; \mathbf{H} \bar{\mathbf{x}}, d^2 \mathbf{I}_{mt}),$$

which defines the likelihood function. This way, the conditional density

$$p(\bar{\mathbf{y}}, \bar{\mathbf{x}} | \theta) = p(\bar{\mathbf{y}} | \bar{\mathbf{x}}, \theta) p(\bar{\mathbf{x}} | \theta)$$

in the joint posterior density (59) takes the form

$$\begin{aligned} p(\bar{\mathbf{y}}, \bar{\mathbf{x}} | \theta) &= (2\pi)^{-m(t+1)/2 - nt/2} a^{-m(t+1)} d^{-nt} \det(\mathbf{A}_\theta) \exp(h(\bar{\mathbf{y}}, \bar{\mathbf{x}}, \theta)) \\ &= (2\pi)^{-m(t+1)/2 - nt/2} a^{-mt} d^{-nt} \exp(h(\bar{\mathbf{y}}, \bar{\mathbf{x}}, \theta)) \end{aligned} \quad (62)$$

as $\det(\mathbf{A}_\theta) = a^m$, where

$$h(\bar{\mathbf{y}}, \bar{\mathbf{x}}, \theta) = -\frac{1}{2a^2} \bar{\mathbf{x}}^\top (\mathbf{A}_\theta^\top \mathbf{A}_\theta) \bar{\mathbf{x}} - \frac{1}{2d^2} (\bar{\mathbf{y}} - \mathbf{H} \bar{\mathbf{x}})^\top (\bar{\mathbf{y}} - \mathbf{H} \bar{\mathbf{x}}).$$

Since the function $h(\bar{\mathbf{y}}, \bar{\mathbf{x}}, \boldsymbol{\theta})$ is quadratic in $\bar{\mathbf{x}}$, the function $\exp(h(\bar{\mathbf{y}}, \bar{\mathbf{x}}, \boldsymbol{\theta}))$ is proportional to a Gaussian density $\mathcal{N}(\bar{\mathbf{x}}; \bar{\boldsymbol{\mu}}_{\boldsymbol{\theta}, \bar{\mathbf{y}}}, \bar{\boldsymbol{\Sigma}}_{\boldsymbol{\theta}})$ with the covariance matrix and the mean vector in the form of

$$\bar{\boldsymbol{\Sigma}}_{\boldsymbol{\theta}} = \left(\frac{1}{a^2} \mathbf{A}_{\boldsymbol{\theta}}^{\top} \mathbf{A}_{\boldsymbol{\theta}} + \frac{1}{d^2} \mathbf{H}^{\top} \mathbf{H} \right)^{-1} \quad \text{and} \quad \bar{\boldsymbol{\mu}}_{\boldsymbol{\theta}, \bar{\mathbf{y}}} = \bar{\boldsymbol{\Sigma}}_{\boldsymbol{\theta}} \left(\frac{1}{d^2} \mathbf{H}^{\top} \bar{\mathbf{y}} \right), \quad (63)$$

respectively. The normalized density function of $\mathcal{N}(\bar{\mathbf{x}}; \bar{\boldsymbol{\mu}}_{\boldsymbol{\theta}, \bar{\mathbf{y}}}, \bar{\boldsymbol{\Sigma}}_{\boldsymbol{\theta}})$ takes the form

$$\mathcal{N}(\bar{\mathbf{x}}; \bar{\boldsymbol{\mu}}_{\boldsymbol{\theta}, \bar{\mathbf{y}}}, \bar{\boldsymbol{\Sigma}}_{\boldsymbol{\theta}}) = (2\pi)^{-m(t+1)/2} \det(\bar{\boldsymbol{\Sigma}}_{\boldsymbol{\theta}})^{-1/2} \exp \left(-\frac{1}{2} (\bar{\mathbf{x}} - \bar{\boldsymbol{\mu}}_{\boldsymbol{\theta}, \bar{\mathbf{y}}})^{\top} \bar{\boldsymbol{\Sigma}}_{\boldsymbol{\theta}}^{-1} (\bar{\mathbf{x}} - \bar{\boldsymbol{\mu}}_{\boldsymbol{\theta}, \bar{\mathbf{y}}}) \right). \quad (64)$$

Using (62)–(64), the ratio of the joint density $p(\bar{\mathbf{y}}, \bar{\mathbf{x}} | \boldsymbol{\theta})$ to $\mathcal{N}(\bar{\mathbf{x}}; \bar{\boldsymbol{\mu}}_{\boldsymbol{\theta}, \bar{\mathbf{y}}}, \bar{\boldsymbol{\Sigma}}_{\boldsymbol{\theta}})$ can be expressed as

$$\frac{p(\bar{\mathbf{y}}, \bar{\mathbf{x}} | \boldsymbol{\theta})}{\mathcal{N}(\bar{\mathbf{x}}; \bar{\boldsymbol{\mu}}_{\boldsymbol{\theta}, \bar{\mathbf{y}}}, \bar{\boldsymbol{\Sigma}}_{\boldsymbol{\theta}})} = (2\pi)^{-nt/2} a^{-mt} d^{-nt} \det(\bar{\boldsymbol{\Sigma}}_{\boldsymbol{\theta}})^{1/2} \exp \left(\frac{1}{2} (\bar{\boldsymbol{\mu}}_{\boldsymbol{\theta}, \bar{\mathbf{y}}}^{\top} \bar{\boldsymbol{\Sigma}}_{\boldsymbol{\theta}}^{-1} \bar{\boldsymbol{\mu}}_{\boldsymbol{\theta}, \bar{\mathbf{y}}} - \frac{1}{d^2} \bar{\mathbf{y}}^{\top} \bar{\mathbf{y}}) \right), \quad (65)$$

which is independent of $\bar{\mathbf{x}}$. Thus, the marginal likelihood (61) can be expressed as

$$p(\bar{\mathbf{y}} | \boldsymbol{\theta}) = \int \frac{p(\bar{\mathbf{y}}, \bar{\mathbf{x}} | \boldsymbol{\theta})}{\mathcal{N}(\bar{\mathbf{x}}; \bar{\boldsymbol{\mu}}_{\boldsymbol{\theta}, \bar{\mathbf{y}}}, \bar{\boldsymbol{\Sigma}}_{\boldsymbol{\theta}})} \mathcal{N}(\bar{\mathbf{x}}; \bar{\boldsymbol{\mu}}_{\boldsymbol{\theta}, \bar{\mathbf{y}}}, \bar{\boldsymbol{\Sigma}}_{\boldsymbol{\theta}}) d\bar{\mathbf{x}} = \frac{p(\bar{\mathbf{y}}, \bar{\mathbf{x}} | \boldsymbol{\theta})}{\mathcal{N}(\bar{\mathbf{x}}; \bar{\boldsymbol{\mu}}_{\boldsymbol{\theta}, \bar{\mathbf{y}}}, \bar{\boldsymbol{\Sigma}}_{\boldsymbol{\theta}})}. \quad (66)$$

Following (63), the quadratic term within the exponential function of the ratio (65) can be expressed as

$$\begin{aligned} \frac{1}{2} (\bar{\boldsymbol{\mu}}_{\boldsymbol{\theta}, \bar{\mathbf{y}}}^{\top} \bar{\boldsymbol{\Sigma}}_{\boldsymbol{\theta}}^{-1} \bar{\boldsymbol{\mu}}_{\boldsymbol{\theta}, \bar{\mathbf{y}}} - \frac{1}{d^2} \bar{\mathbf{y}}^{\top} \bar{\mathbf{y}}) &= \frac{1}{2d^2} \bar{\mathbf{y}}^{\top} (\mathbf{H} \bar{\boldsymbol{\mu}}_{\boldsymbol{\theta}, \bar{\mathbf{y}}} - \bar{\mathbf{y}}) \\ &= \frac{1}{2d^2} \bar{\mathbf{y}}^{\top} \left(\frac{1}{d^2} \mathbf{H} \bar{\boldsymbol{\Sigma}}_{\boldsymbol{\theta}} \mathbf{H}^{\top} - \mathbf{I}_{nt} \right) \bar{\mathbf{y}} \end{aligned}$$

Thus, the marginal likelihood (61) takes the form

$$p(\bar{\mathbf{y}} | \boldsymbol{\theta}) = (2\pi)^{-nt/2} a^{-mt} d^{-nt} \det(\bar{\boldsymbol{\Sigma}}_{\boldsymbol{\theta}})^{1/2} \exp \left(-\frac{1}{2d^2} \bar{\mathbf{y}}^{\top} \left(\mathbf{I}_{nt} - \frac{1}{d^2} \mathbf{H} \bar{\boldsymbol{\Sigma}}_{\boldsymbol{\theta}} \mathbf{H}^{\top} \right) \bar{\mathbf{y}} \right),$$

where the matrix $(\mathbf{I}_{nt} - \frac{1}{d^2} \mathbf{H} \bar{\boldsymbol{\Sigma}}_{\boldsymbol{\theta}} \mathbf{H}^{\top})$ is positive semidefinite by the Woodbury formula. Then, the explicit form of the posterior parameter density follows from (60).

References

Brian D O Anderson and John B Moore. *Optimal filtering*. Courier Corporation, 2012.

Christophe Andrieu, Arnaud Doucet, and Roman Holenstein. Particle Markov chain Monte Carlo methods. *Journal of the Royal Statistical Society: Series B (Statistical Methodology)*, 72(3):269–342, 2010.

Alexandros Beskos, Ajay Jasra, Nikolas Kantas, and Alexandre Thiery. On the convergence of adaptive sequential Monte Carlo methods. *Annals of Applied Probability*, 26(2):1111–1146, 2016.

Daniele Bigoni, Allan P Engsig-Karup, and Youssef M Marzouk. Spectral tensor-train decomposition. *SIAM Journal on Scientific Computing*, 38(4):A2405–A2439, 2016.

Yoram Bresler. Two-filter formulae for discrete-time non-linear Bayesian smoothing. *International Journal of Control*, 43(2):629–641, 1986.

Mark Briers, Arnaud Doucet, and Simon Maskell. Smoothing algorithms for state-space models. *Annals of the Institute of Statistical Mathematics*, 62:61–89, 2010.

Hans-Joachim Bungartz and Michael Griebel. Sparse grids. *Acta numerica*, 13:147–269, 2004.

Olivier Cappé, Eric Moulines, and Tobias Rydén. *Inference in Hidden Markov Models*. Springer Science & Business Media, 2006.

James Carpenter, Peter Clifford, and Paul Fearnhead. Improved particle filter for nonlinear problems. *IEE Proceedings-Radar, Sonar and Navigation*, 146(1):2–7, 1999.

Nan Chen and Andrew J Majda. Conditional Gaussian systems for multiscale nonlinear stochastic systems: Prediction, state estimation and uncertainty quantification. *Entropy*, 20(7):509, 2018.

Nan Chen, Andrew J Majda, and Xin T Tong. Rigorous analysis for efficient statistically accurate algorithms for solving Fokker–Planck equations in large dimensions. *SIAM/ASA Journal on Uncertainty Quantification*, 6(3):1198–1223, 2018.

Nan Chen, Yingda Li, and Honghu Liu. Conditional Gaussian nonlinear system: A fast preconditioner and a cheap surrogate model for complex nonlinear systems. *Chaos: An Interdisciplinary Journal of Nonlinear Science*, 32(5):053122, 2022.

Nicolas Chopin, Pierre E Jacob, and Omiros Papaspiliopoulos. SMC2: an efficient algorithm for sequential analysis of state space models. *Journal of the Royal Statistical Society: Series B (Statistical Methodology)*, 75(3):397–426, 2013.

Alexandre J Chorin and Xuemin Tu. Implicit sampling for particle filters. *Proceedings of the National Academy of Sciences*, 106(41):17249–17254, 2009.

Gregory M Constantine and Thomas H Savits. A multivariate Faa di Bruno formula with applications. *Transactions of the American Mathematical Society*, 348(2):503–520, 1996.

Dan Crisan and Joaquin Miguez. Nested particle filters for online parameter estimation in discrete-time state-space Markov models. *Bernoulli*, 24(4A):3039–3086, 2018.

Tiangang Cui and Sergey Dolgov. Deep composition of tensor-trains using squared inverse Rosenblatt transports. *Foundations of Computational Mathematics*, 22(6):1863–1922, 2022.

Tiangang Cui and Xin T Tong. A unified performance analysis of likelihood-informed subspace methods. *Bernoulli*, 28(4):2788–2815, 2022.

Tiangang Cui, James Martin, Youssef M. Marzouk, Antti Solonen, and Alessio Spantini. Likelihood-informed dimension reduction for nonlinear inverse problems. *Inverse Problems*, 30:114015, 2014.

Tiangang Cui, Sergey Dolgov, and Olivier Zahm. Self-reinforced polynomial approximation methods for concentrated probability densities. *arXiv preprint: 2303.02554*, 2023.

Ingrid Daubechies. *Ten lectures on wavelets*. SIAM, 1992.

Carl de Boor, Ronald A DeVore, and Amos Ron. On the construction of multivariate (pre) wavelets. *Constructive approximation*, 9(2):123–166, 1993.

Pierre Del Moral, Arnaud Doucet, and Ajay Jasra. On adaptive resampling strategies for sequential Monte Carlo methods. *Bernoulli*, 18(1):252–278, 2012.

Ronald A DeVore and Vasil A Popov. Interpolation of besov spaces. *Transactions of the American Mathematical Society*, 305(1):397–414, 1988.

Josef Dick, Frances Y Kuo, and Ian H Sloan. High-dimensional integration: the quasi-Monte Carlo way. *Acta Numerica*, 22:133–288, 2013.

Sergey V Dolgov and Dmitry V Savostyanov. Alternating minimal energy methods for linear systems in higher dimensions. *SIAM Journal on Scientific Computing*, 36(5):A2248–A2271, 2014.

Arnaud Doucet and Adam M Johansen. A tutorial on particle filtering and smoothing: Fifteen years later. *Handbook of nonlinear filtering*, 12(656-704):3, 2009.

Dinh Dũng, Vladimir Temlyakov, and Tino Ullrich. *Hyperbolic cross approximation*. Springer, 2018.

Garry A Einicke and Langford B White. Robust extended Kalman filtering. *IEEE Transactions on Signal Processing*, 47(9):2596–2599, 1999.

Geir Evensen. The ensemble Kalman filter: Theoretical formulation and practical implementation. *Ocean Dynamics*, 53(4):343–367, 2003.

Geir Evensen, Femke C Vossepoel, and Peter Jan van Leeuwen. *Data assimilation fundamentals: A unified formulation of the state and parameter estimation problem*. Springer Nature, 2022.

Paul Fearnhead, David Wyncoll, and Jonathan Tawn. A sequential smoothing algorithm with linear computational cost. *Biometrika*, 97(2):447–464, 2010.

Andrew Gelman and Xiao-Li Meng. Simulating normalizing constants: From importance sampling to bridge sampling to path sampling. *Statistical Sciences*, pages 163–185, 1998.

Mathieu Gerber and Nicolas Chopin. Sequential quasi Monte Carlo. *Journal of the Royal Statistical Society Series B: Statistical Methodology*, 77(3):509–579, 2015.

Walter R Gilks and Carlo Berzuini. Following a moving target—Monte Carlo inference for dynamic Bayesian models. *Journal of the Royal Statistical Society: Series B (Statistical Methodology)*, 63(1):127–146, 2001.

Simon J Godsill, Arnaud Doucet, and Mike West. Monte Carlo smoothing for nonlinear time series. *Journal of the American Statistical Association*, 99(465):156–168, 2004.

Neil J Gordon, David J Salmond, and Adrian FM Smith. Novel approach to nonlinear/non-Gaussian Bayesian state estimation. In *IEEE Proceedings F (Radar and Signal Processing)*, volume 140, pages 107–113. IET, 1993.

Alex Gorodetsky, Sertac Karaman, and Youssef M Marzouk. A continuous analogue of the tensor-train decomposition. *Computer Methods in Applied Mechanics and Engineering*, 347:59–84, 2019.

Georg A Gottwald and Sebastian Reich. Combining machine learning and data assimilation to forecast dynamical systems from noisy partial observations. *Chaos: An Interdisciplinary Journal of Nonlinear Science*, 31(10):101103, 2021.

Michael Griebel and Helmut Harbrecht. Analysis of tensor approximation schemes for continuous functions. *Foundations of Computational Mathematics*, 23:219–240, 2023.

Wolfgang Hackbusch. *Tensor spaces and numerical tensor calculus*, volume 42. Springer Science & Business Media, 2012.

Edward Herbst and Frank Schorfheide. Tempered particle filtering. *Journal of Econometrics*, 210(1):26–44, 2019.

Truong-Vinh Hoang, Sebastian Krumscheid, Hermann G Matthies, and Raúl Tempone. Machine learning-based conditional mean filter: a generalization of the ensemble Kalman filter for nonlinear data assimilation. *arXiv preprint: 2106.07908*, 2021.

Rudolph Emil Kalman. A new approach to linear filtering and prediction problems. 1960.

Nicholas Kantas, Arnaud Doucet, Sumeetpal Sindhu Singh, and Jan Marian Maciejowski. An overview of sequential Monte Carlo methods for parameter estimation in general state-space models. *IFAC Proceedings Volumes*, 42(10):774–785, 2009.

Nikolas Kantas, Alexandros Beskos, and Ajay Jasra. Sequential Monte Carlo methods for high-dimensional inverse problems: A case study for the navier–stokes equations. *SIAM/ASA Journal on Uncertainty Quantification*, 2(1):464–489, 2014.

Genshiro Kitagawa. Monte Carlo filter and smoother for non-Gaussian nonlinear state space models. *Journal of Computational and Graphical Statistics*, 5(1):1–25, 1996.

Genshiro Kitagawa and Seisho Sato. Monte Carlo smoothing and self-organising state-space model. *Sequential Monte Carlo methods in practice*, pages 177–195, 2001.

Herbert Knothe et al. Contributions to the theory of convex bodies. *The Michigan Mathematical Journal*, 4(1):39–52, 1957.

Jun S Liu, Rong Chen, and Tanya Logvinenko. A theoretical framework for sequential importance sampling with resampling. In *Sequential Monte Carlo methods in practice*, pages 225–246. Springer, 2001.

Stephane G Mallat. Multiresolution approximations and wavelet orthonormal bases of $L^2(\mathbb{R})$. *Transactions of the American Mathematical Society*, 315(1):69–87, 1989.

Simon Maskell and Neil Gordon. A tutorial on particle filters for on-line nonlinear/non-Gaussian Bayesian tracking. *IEEE Target Tracking: Algorithms and Applications (Ref. No. 2001/174)*, pages 2–1, 2002.

Isambi S Mbalawata, Simo Särkkä, and Heikki Haario. Parameter estimation in stochastic differential equations with Markov chain Monte Carlo and non-linear Kalman filtering. *Computational Statistics*, 28:1195–1223, 2013.

Matthias Morzfeld, Xuemin Tu, Ethan Atkins, and Alexandre J Chorin. A random map implementation of implicit filters. *Journal of Computational Physics*, 231(4):2049–2066, 2012.

Jimmy Olsson, Olivier Cappé, Randal Douc, and Éric Moulines. Sequential Monte Carlo smoothing with application to parameter estimation in nonlinear state space models. *Bernoulli*, 14(1):155–179, 2008.

Ivan Oseledets and Eugene Tyrtyshnikov. TT-cross approximation for multidimensional arrays. *Linear Algebra and its Applications*, 432(1):70–88, 2010.

Ivan V Oseledets. Tensor-train decomposition. *SIAM Journal on Scientific Computing*, 33(5):2295–2317, 2011.

Hill Peter D. Kernel estimation of a distribution function. *Communications in Statistics-Theory and Methods*, 14(3):605–620, 1985.

Michael K Pitt and Neil Shephard. Filtering via simulation: Auxiliary particle filters. *Journal of the American Statistical Association*, 94(446):590–599, 1999.

Michael K Pitt and Neil Shephard. Auxiliary variable based particle filters. *Sequential Monte Carlo methods in practice*, pages 273–293, 2001.

Sebastian Reich. A nonparametric ensemble transform method for Bayesian inference. *SIAM Journal on Scientific Computing*, 35(4):A2013–A2024, 2013.

Sebastian Reich and Colin Cotter. *Probabilistic forecasting and Bayesian data assimilation*. Cambridge University Press, 2015.

Paul B Rohrbach, Sergey Dolgov, Lars Grasedyck, and Robert Scheichl. Rank bounds for approximating Gaussian densities in the tensor-train format. *SIAM/ASA Journal on Uncertainty Quantification*, 10(3):1191–1224, 2022.

Murray Rosenblatt. Remarks on a multivariate transformation. *The Annals of Mathematical Statistics*, 23(3):470–472, 1952.

Simo Särkkä. *Bayesian filtering and smoothing*. Number 3. Cambridge University Press, 2013.

Simo Särkkä, Jouni Hartikainen, Isambi Sailon Mbalawata, and Heikki Haario. Posterior inference on parameters of stochastic differential equations via non-linear Gaussian filtering and adaptive mcmc. *Statistics and Computing*, 25(2):427–437, 2015.

Jie Shen, Tao Tang, and Li-Lian Wang. *Spectral methods: algorithms, analysis and applications*, volume 41. Springer Science & Business Media, 2011.

Bernard W Silverman. *Density estimation for statistics and data analysis*, volume 26. CRC press, 1986.

Chris Snyder, Thomas Bengtsson, Peter Bickel, and Jeff Anderson. Obstacles to high-dimensional particle filtering. *Monthly Weather Review*, 136(12):4629–4640, 2008.

Alessio Spantini, Daniele Bigoni, and Youssef Marzouk. Inference via low-dimensional couplings. *The Journal of Machine Learning Research*, 19(1):2639–2709, 2018.

Alessio Spantini, Ricardo Baptista, and Youssef Marzouk. Coupling techniques for nonlinear ensemble filtering. *SIAM Review*, 64(4):921–953, 2022.

Andrew M Stuart. Inverse problems: a Bayesian perspective. *Acta Numerica*, 19:451–559, 2010.

Holger Wendland. *Scattered data approximation*, volume 17. Cambridge university press, 2004.

Christopher KI Williams and Carl Edward Rasmussen. *Gaussian processes for machine learning*, volume 2. MIT press Cambridge, MA, 2006.

Dongbin Xiu and George Em Karniadakis. The wiener–askey polynomial chaos for stochastic differential equations. *SIAM Journal on Scientific Computing*, 24(2):619–644, 2002.

Olivier Zahm, Tiangang Cui, Kody Law, Alessio Spantini, and Youssef Marzouk. Certified dimension reduction in nonlinear bayesian inverse problems. *Mathematics of Computation*, 91(336):1789–1835, 2022.